

UNMELTED COSMIC METAL PARTICLES IN THE INDIAN OCEAN

M. Shyam Prasad*, N.G. Rudraswami, Agnelo A. De Araujo and Vijay D. Khedekar

*shyam@nio.org

CSIR-National Institute of Oceanography,
Dona Paula, Goa – 403004, INDIA

Abstract

Fe-Ni metal is a common constituent of most meteorites and is an indicator of the thermal history of the respective meteorites, it is a diagnostic tool to distinguish between groups/sub-groups of meteorites. In spite of over a million micrometeorites collected from various domains, reports of pure metallic particles among micrometeorites have been extremely rare. We report here the finding of a variety of cosmic metal particles such as kamacite, plessite, taenite, and Fe-Ni beads from deepsea sediments of the Indian Ocean, a majority of which have entered the Earth unaffected by frictional heating during atmospheric entry. Such particles are known as components of meteorites but have never been found as individual entities. Their compositions suggest precursors from a variety of meteorite groups, thus providing an insight into the metal fluxes on the Earth. Some particles have undergone heating and oxidation to different levels during entry developing features similar to I-type cosmic spherules, suggesting atmospheric processing of individual kamacites/taenite grains as another hitherto unknown source for the I-type spherules. The particles have undergone post-depositional aqueous alteration transforming finally into the serpentine mineral cronstedtite. Aqueous alteration products of kamacite reflect the local micro-environment, therefore they have the potential to provide information on the composition of water in the solar nebula, on the parent bodies or on surfaces of planetary bodies. Our observations suggest it would take sustained burial in water for tens of thousands of years under cold conditions for kamacites to alter to cronstedtite.

INTRODUCTION

Metal in the form of Fe-Ni beads occurring in all the three basic types of cosmic spherules (I-type, G-type and the S-type) have been reported from many micrometeorite collections Blanchard et al., (1980); Genge and Grady (1997; 1998); Taylor et al. (2000); Cordier et al. (2011); Rudraswami et al. (2014a). The finding of unmelted metallic particles is rare. Maurette et al. (1987) described unmelted metal from Greenland cryoconite collections comprising of 0.5% of the components, these particles were identified as primary, rather than ablation products of larger meteorites. Robin et al. (1988) suggested that the irregular Fe-Ni metallic particles could be the parent bodies of I-type spherules in view of their similar elemental ratios. Badjukov et al. (2009) reported two unmelted metallic particles (kamacite and taenite) from Novaya Zemlya glacier. They suggested that iron meteorites cannot be the precursors for these particles.

The known cosmic sources of metals on Earth comprise of the I-type and the G-type spherules which form ~2-5% of unbiased micrometeorite collections (Blanchard et al., 1980; Prasad et al., 2013; Taylor et al., 2000); rare reports of unmelted metal (Maurette et al. 1987) and meteoric smoke which are metals released in the troposphere due to the vaporization of meteoroids (Plane, 2012). Not many investigations have been carried out to identify the contribution of metals from extraterrestrial sources on the Earth. Some of the metal is processed and released in the Earth's atmosphere as Fe-Ni beads (Brownlee et al. 1984; Genge and Grady, 1997; Rudraswami et al. 2014a; 2014b). The refractory PGE/palladium ratios of the Fe-Ni beads in I-

type, G-type and also in S-type spherules have been identified to be chondritic (Rudraswami et

al. 2014a). In addition, there are strong arguments in favor of cosmic metallic particles entering the Earth in their primary forms (Herzog et al. 1999). The larger-sized cosmic spherules would especially undergo the immiscible Fe-Ni bead separation during entry. Based on the size estimates of dust-sized cosmic material entering the Earth, Genge and Grady (1998) suggested ~6% of all incoming particles would produce Fe-Ni beads which would have approximate sizes of <30 μm diameters. Brownlee and Hodge (1973) described Fe-Ni and Fe-Ni-S spheres collected in the stratosphere which had small diameters (<10 μm). They suggested that these particles are ablation debris from millimetre meteoroids or in view of their high sulphur contents they could have been parts of troilite dislodged from chondritic meteorites. Rochette et al. (2009) investigated large (>400 μm) I-type spherules from Antarctica, they found that there are similarities in the Ni/Co ratios of these spherules with those of chondritic kamacite. Therefore, they suggested that chondritic kamacites could be the precursors for some of the large I-type spherules.

We report here the discovery of a hitherto unknown variety of metallic particles of cosmic origin recovered by raking the deep seafloor of the Indian Ocean with a magnet-impregnated dredge. We present here their compositions and infer the possible parent bodies. The particles appear to be released from the asteroid belt due to collisions and entered the Earth in an unmelted form. Their compositions suggest precursors from a variety of meteorite groups, thus providing an insight into the metal fluxes on the Earth. Therefore, the present finding enlarges the inventory of unmelted metal particles from extraterrestrial sources. The particles display evidences for atmospheric entry and also post-depositional alteration during their residence time on the seafloor. These particles have been resting on the seafloor over a range of residence times and have undergone aqueous alteration to different extents in a known environment. The metal particles in this study also provide ground truth for understanding long term hydration of metal particles, these can be analogs for aqueous alteration in cold, silica-rich, alkaline conditions on planetary surfaces.

SAMPLE COLLECTION AND METHODS

Six bar magnets (1400 gauss intensity) were placed together on an aluminium plate, and were fastened with a mesh. A bolting cloth was placed above this mesh. This assembly was fixed to a dredge which was dragged along the seafloor in the Central Indian Ocean at water depths of ~5200 metres. The sampling operations were carried out during two cruises of 35-day duration each onboard AASidorenko (Cruise Nos. AAS-26 (May-June, 2000) and AAS-27 (July-August 2000) a research vessel chartered by the Govt. of India. While on the seafloor, the dredge was dragged for ~10-15 minutes and was lifted to a height of 50 metres above the seafloor to allow the accumulated sediments to be washed down. It was subsequently lowered and was dragged again for 15 minutes. This cycle of dragging and lifting was repeated for 10 times before the dredge was hauled up onboard the vessel. Each sampling operation was for a duration of 12 hours and the distance travelled on the seafloor during this time by the dredge is about 4 km. The material attracted by the magnetic assembly came from the sediment ploughed by the dredge. The magnetic material recovered was carefully washed with distilled water in the lab, and was dried at 40⁰C in the oven and stored in petri dishes. The material comprised of spherules, black and orange colored particles mostly of volcanogenic origin. The spherules were hand-picked from the dried magnetic materials under a binocular microscope and were mounted in epoxy as per their sizes. The rest of the magnetic material recovered from four such sampling operations was mounted in several epoxy mounts as per sizes of the materials and polished sections of a total number of 10087 magnetic particles were examined in SEM-EDS and analyzed with the EPMA for cosmic particulate matter. The cosmic

particles were identified based on their textures, and chemical compositions as established in previous investigations (Blanchard et al., 1980; Genge et al. 2007; Folco and Cordier, 2015).

The metal micrometeorites were identified as cosmic especially on the basis of their Fe, Ni and Co contents. The metal micrometeorites in view of their higher atomic numbers had higher signal intensities in the backscattered (BSE) mode of the SEM, this facilitated their recognition. A JEOL JSM 5800LV SEM with OXFORD ISIS EDS (at CSIR- National Institute of Oceanography, India) was used for analysis and for high resolution imaging, and a CAMECA SX-5 EPMA (at CSIR- National Institute of Oceanography, Goa, India) was used for quantitative analysis of the cosmic particles. The system has four spectrometers and the analyses were carried at an acceleration voltage of 15 kV, a beam current of 12nA and at a beam diameter of $\sim 2\mu\text{m}$. The standards used for calibrations were Jadeite for Na, Diopside for Mg, Olivine for Si, Apatite for P, Pentlandite for S, Orthoclase for K, Plagioclase for Ca, Benitoite for Ti, Pure Vanadium for V, Crocoite for Cr, Bustamite for Mn, Magnetite for Fe, Skutterudite for Co, and Pentlandite for Ni. The error percentages for the results obtained were within 1-2%. X - ray imaging was carried out using 15 KV accelerating voltage and a beam current of 20 nA with a D time of 100 msec and resolution of 512 X 512 pixels. The data reduction and corrections were done using the PAP model (Pouchou & Pichoir, 1991).

Hydrated minerals presented low totals in the EPMA. They contain H which is not detected by the system. We kept a cut off at 70% totals for the hydrated parts of the particles. A similar cut off has been presented by Palmer and Lauretta, (2011) for hydrated kamacites.

The hydrated particles investigated here were not completely altered or else it would have been very difficult to recognize them. A close parallel is the PCPs (poorly characterised particles) observed in meteorites. Complete hydration of Fe-Ni particles would give them low reflectivity in the BSE mode and they would be indistinguishable among the terrestrial particles. We have taken care to analyse the least altered portions of all the particles. For presenting maximum effects of hydration we have analysed the most hydrated parts of the particles. It is easier to spot the partly altered ones because the unaltered Fe-Ni portions of these particles show higher signal intensity in the backscattered mode (Figs.1,2, 3).

RESULTS

Description of metal micrometeorites

We examined polished sections of 10,087 particles in the SEM and the EPMA. Out of these, >800 particles are melted micrometeorites and ~ 120 particles are unmelted silicate particles which are not

dealt in this investigation. One hundred and twenty nine particles are unmelted metal which are investigated here. They comprise of the following types :

kamacite (52), Plessite (10), Taenite (17) (Fig.1); Fe-Ni beads (50) (Fig. 2).

The chemical compositions of the kamacites, plessites, taenites are presented in Table 1. Since many of them contain oxide rims, the rim compositions are also determined and the results are presented in Table 2. The compositions of unoxidized beads are presented in Table 3 and that of oxidized beads in Table 4. Many particles from all the above categories have undergone aqueous alteration while they were on the seafloor, the chemical compositions of the altered portions are presented in Table 5.

Kamacite, plessite and taenite are in monocrystalline forms (Fig.1; Table 1), i.e., they are present as individual mineral grains. Generally, these minerals are observed together in polycrystalline forms in meteorites (Brearley and Jones, 1998; Bevan and Axon, 1980). The largest kamacite particle (AAS26-D37-M14P4, Fig. 1) has a size of ~400 μm . There are a few particles that have sizes ~300 μm (eg. AAS27-D6-MT7-P9). These particles are surrounded by an oxide rim and they also show aqueous alteration (Fig. 1). The smallest kamacite has dimensions of 14 X 25 μm . A majority of the particles are in the size range of 50-80 μm .

They vary in shapes from subhedral to irregular. The quantity of heating undergone during entry is discernible by their shapes : there are those which are angular in shape and do not show signs of any heating during atmospheric entry (e.g. Fig. 1). The particles that have undergone minimal heating and oxidation during entry have developed magnetite rims (rim thickness : ~2 - 7.3 μm : Table 2; Fig.1b-f).. These rims sometimes display two phases of oxidation : an outer magnetite and inner wustite (Fig. 1 c-f), both these layers contain low nickel (Table 2). Particles such as these still retain their crystalline shapes (Fig. 1b,c). With greater heating the particles lose their original crystallinity and attain spherical shapes (Fig. 1 E).

Taenites are mostly in sub-hedral or even euhedral forms (Fig.1a,b). The rims on taenites are not as thick as on the kamacites. The taenites show a large variation in their Ni contents generally from ~5% to ~20% in some particles (Table 1; Table S1 supplement). The dimensions of the particles are similar to those of the kamacites. Plessites are identified based on their nickel percentages between 10- 20% (Table 1). In meteorites plessite occurs as an intergrowth of kamacite and taenite. It is a two phase mixture of kamacite and taenite (Brearley and Jones, 1998). In the present study, plessite is observed as individual mineral grains (Fig. 1f).

Fifty Fe-Ni beads are identified in this study. The Fe-Ni beads have generally small diameters ($\leq 50\mu\text{m}$). One such bead has a diameter of 294 μm , it is surrounded by an oxidized rim in which fine

distinction can be made between the outer magnetite and inner wustite (Fig.1g). There is no chemical zoning in this particle, it shows uniform Ni content of ~10%, therefore it has cooled extremely fast and appears to have formed during atmospheric entry. This is the case for all the Fe-Ni beads, they all have homogeneous Fe and Ni contents. The beads are either oxidized or unoxidized (Fig. 2; Tables 3, 4). Some of the beads have kamacitic Fe:Ni ratios (Table 3). They are comprised of Fe, Ni and Co. The Ni contents in the beads show a large variation from ~5% to 68%, there is no general trend with respect to size of the spherule, bead size in relation with the nickel contents. The range of Ni seen in these beads overlaps those analysed in the beads found in cosmic spherules of all the three basic types (Rudraswami et al., 2014a). The oxidized beads have lower reflectivity and display several cracks (Fig. 2 E,F,G). These cracks could have developed while these particles on the seafloor due to the absorption of oxygen by Fe which is a redox sensitive element. The Ni contents of the oxidized beads (Table 4) are also much lower than those which are not oxidized (Table 3). This phenomenon could be a beginning of aqueous alteration described in a later section.

In addition, we found >800 spherules of which the metal-rich spherules (I-type and G-type) are dominant. Almost 50% of the spherules are of either I or G-type. The others are of s-type which have textures that are barred, porphyritic, cryptocrystalline, glassy etc. One metal bead (Fig. 1g) which is also has the largest diameter among beads in this collection shows an oxidized shell of magnetite/wustite. Mostly, the smaller-sized I-type spherules $\leq 100\mu\text{m}$ comprise dominantly of an Fe-Ni bead with a thin rim of oxidized metal (Fig. 3a,b), the rim diameter increases with increase in size of the I-type spherules and the oxidation is much more prominent, where the magnetite and wustite phases are discernible more clearly (Fig. 3 c-e). The thickness of the oxidized layers seems to increase systematically with increased levels of heating and oxidation. What were initial layers of magnetite and wustite now progressively form interlocking crystals of magnetite and wustite in a myrmekite-like texture. Further heating and oxidation leads to the spherule being dominated by magnetites where the noble, unoxidizable elements segregate to form platinum group nuggets (Fig. 3f) (Brownlee et al. 1984). The I-type spherules appear to evolve systematically from the beads with increasing heating and oxidation.

Aqueous alteration

Many particles show signs of aqueous alteration. The particles have been residing on the seafloor for varying amounts of time and have been interacting with the local environment continuously. The alteration is seen in the form of dull texture seen in the altered parts of the particles. The Fe-Ni portions of the particles seem to alter to more easily than the oxidized rims (Fig. 7). The chemical

changes undergone as a result of these low temperature alterations are the addition of water to the structure which causes it to expand in size and the EPMA totals of the altered portions are therefore low because the system cannot detect water. Further, there is a progressive increase in the addition of lithophile elements such as Si, Mg, Ca, and also Al from the local medium. During the initial stages of alteration, the appearance of tracks from the periphery inwards are observed (Fig. 7a), with greater exposure to the seafloor environment larger areas of the Fe-Ni portions appear to be altered with concomitant increase in the lithophile contents and decrease in Ni contents in these portions (Table 5). The more advanced stages of alteration show desiccation cracks (Fig. 7D) and fibrous structures (Fig. 7e, f) which are typically seen in kamacites which have undergone serpentinization due to aqueous alteration (Palmer, 2011). It is conceivable that with complete alteration the entire particle would become dull textured with substantial loss of nickel and in appearance would resemble poorly characterized phases or PCPs observed in carbonaceous chondrites (Brearley and Jones, 1998). On the ternary diagram of Fe-Si-Mg (Tomeoka and Buseck, 1985; Fig. 8) of the altered portions of the particles, it is discernible that there is a progression of aqueous alteration of the particles from a pure kamacite phase to that of the serpentine mineral cronstedtite.

DISCUSSION

The presence of an oxidized rim is considered as an important evidence for deciphering cosmic origin of a particle. Toppani and Libourel (2003) carried out pulse heating experiments on CI chondrite material (Orgueil) at varying oxygen fugacities, heating times and different temperatures. They observed the formation of a rim due to peripheral partial melting of iron-rich material and phyllosilicate phases. This resulted in the formation of a thin shell of oxidized iron comprising of magnetites (or spinels). In the proximity of the rim formation of microcrystals of olivine takes place and also the formation of vesicles due to the release of volatile elements due to heating during entry. Genge (2006) in an extensive investigation documented the presence of such igneous rims generated by surface melting on antarctic micrometeorites, the rims were found to be more prominent on the fine-grained micrometeorites rather than on the coarse-grained micrometeorites. The rims comprising of such a variety of phases is possible because of the heating of inhomogeneous material.

When a metal micrometeorite in the form of an alloy of Fe-Ni experiences heating during entry, high temperature oxidation takes place where the metals experience different levels of oxidation reflecting the respective oxidation states attained during entry, i.e., either divalent or trivalent states of Fe (Kosakevich and Disnar, 1997). If the heating is minimum, this results in the formation of more or less continuous layers from the periphery of the particle inwards that represent different levels of oxidation experienced during entry heating (Blanchard and Davis, 1978). A similar phenomenon is

observed in most of the particles that contain a rim. The rim comprises of two different layers which have compositions similar to those that of wustite and magnetite (Fig 1; Table 2). The outermost part of the particle invariably shows composition of that of magnetite, whereas wustite is always the layer immediately interior to the magnetite. The presence of wustite implies that the particle has passed through a region of very low oxygen fugacity and has attained a temperature of 550 K. Wustite a metastable iron oxide which has stoichiometric proportions of Fe and O can only form under very low oxygen fugacity conditions such as those that exist at the top of Earth's atmosphere, therefore wustite has been considered as one of the primary evidences for the cosmic nature of a metallic particle (Blanchard, 1972; Brownlee, 1981). Blanchard and Davis (1978) simulated atmospheric entry of Fe-Ni alloys using different iron meteorites, they observed skin melting leading to formation of different microlayers of magnetite (outer layer) and wustite (inner layer). With further heating and oxidation these layers developed into myrmekite-like growth of magnetite and wustite as observed in I-type spherules commonly. From the above investigations it appears plausible that the metal micrometeorites in the present study have undergone minimal melting of the outer shells due to heating and oxidation during entry leading to the formation of a magnetite-wustite shell. With progressive heating and oxidation they would be transformed into I-type spherules comprising of interwoven magnetite and wustite.

The issue in question is that of the effects of size during atmospheric entry. It is interesting to note that several recent investigations have presented unmelted particles of with dimensions of 500 – 2000 μm (van Ginneken et al. 2012; Rochette et al., 2008), some of these particles contained oxidized shells either partially or fully enveloping them. Dynamic entry models suggest that the largest particles that could enter the Earth unmelted could be up to 300 – 400 μm , however, these enter under extreme conditions of very low entry angles and reach the Earth's surface with minimum heating and oxidation, they constitute <1% of the flux (Love and Brownlee,1993). Therefore, the dynamics of atmospheric entry presents a very narrow window through which such large particles can enter the Earth in an unmelted form. The process of surviving unmelted becomes more difficult in view of high density of particles such as the kamacites/taenites/Fe-Ni beads etc., because their densities provide greater momentum to penetrate deeper into the atmosphere which would lead to greater friction, heating and oxidation. Genge (2016) simulated atmospheric entry of metal particles, his study suggests that the higher density of the Fe-Ni particles would cause them to reach much higher peak temperatures than silicate particles of similar sizes therefore the iron micrometeoroids of sizes greater than 40 μm cannot survive atmospheric entry without melting. These particles however, experience much less mass loss than those experienced by silicate materials because of the

lower evaporation rates of iron oxide liquids. He also suggested that deceleration high in the atmosphere would enable metal bead survival. The only mechanism that can facilitate deceleration is that these particles could be parts of larger material dislodged from the asteroid belt which fragment at the top of the atmosphere. This process would release fragmented particles that would have lost their momentum during entry and would subsequently have lower velocities, less frictional heating enabling even the more silicate particles that contain volatile phases to survive the entry process with minimal skin melting.

The kamacites observed in meteorites are either fully crystalline, partially crystalline or do not have crystalline shapes (Palmer and Lauretta, 2011). They often contain alteration rims where aqueously altered phases comprising serpentine minerals such as the tochilinite or cronstedtite are seen. Also, some of the kamacites/taenites contain tetrataenite rims with enhancement in Ni contents these have developed due to cooling and diffusion of nickel. Rubin et al. (1999) reported many chondrules in Type-3 Ordinary Chondrites (eg. Semarkona) containing FeO-rich chondrules, and FeO-poor chondrules as well. In these chondrules they presented kamacite-grains which are spherical and contained rims of troilite, tetrataenite. They also reported tetrataenite inclusions contained inside kamacites. While we did not find tetrataenite, we found one particle in this collection which has a taenite inclusion (Fig.1E).

The oxidized rims seen on metal particles in this study have developed due to heating and oxidation during entry. Therefore, the differences in the rim compositions between kamacites in the meteorites and those in the present investigation could be due to the atmospheric processing of the kamacites in the present study

Chemical Compositions and Parent Bodies

The Fe:Ni ratios of kamacites in meteorites are 19:1 (Wood, 1967). All the kamacites in this investigation have Fe:Ni ratios close to this ratio (Table 1), therefore are considered here as extraterrestrial. There are no known reports of terrestrial plessites or taenites. Further, Fe-Ni beads are observed solely in melted micrometeorites and have a wide range in Fe-Ni compositions (e.g., Rudraswami et al., 2014a) which do not conform to known meteoritic Fe;Ni ratios. The beads in this investigation have a similar range in Fe-Ni compositions which allow us to consider these particles to be of extraterrestrial origin. The Ni/Co ratios of kamacites are diagnostic of different meteorites or within sub-groups of meteorites as well – this is especially true for ordinary chondrites. Rubin (1990) observed an increase in Co contents and a complementary decrease in the Ni contents of Kamacites from H → L → LL chondrites. He attributed this to the greater oxidisability of Fe relative

to Co which leads to kamacite grains becoming richer in Co as the oxidation state increases from H to L to LL. There are significant differences in Ni/Co variation patterns within the kamacites in ordinary chondrites, between the ordinary chondrites and the kamacites in the carbonaceous chondrites (Smith et al. 1993). Afatalab and Wasson (1980) and Rubin (1990) found a systematic and diagnostic variation in the ranges of Ni and Co in the three chondrite groups. This property enables identification of the chondrite group to which the individual kamacite/taenite belongs.

As pointed out by Wood (1967), the Ni and Co ratios of many kamacites from different meteorites have overlapping compositions (Fig.4). Kamacites from CV, CM, CO, ordinary chondrites, iron and stony irons all have a common area of overlap in composition. There are however some kamacites which show distinct overlap with those from CM chondrites. The Ni:Co ratios of kamacites, plessites and taenites in this investigation seem to be spread over a large area (Fig. 4) encompassing not only those from the carbonaceous chondrites but those from ordinary chondrites (especially those with higher nickel contents such as the plessites and taenites). The high nickel particles do fall in the zones defined by the kamacites from iron, stony iron meteorites, however, these zones also overlap with the ordinary chondrites. Therefore, ordinary chondrites seem to make a distinct contribution among the high nickel metal micrometeorites. This observation is also strengthened by the M-shaped patterns shown by the particles due to slow cooling and diffusion of nickel as discussed in a later chapter. Apparently, the metals in the present collection seem to have been contributed by multiple parent meteorites. Comminution experiments on chondrites have shown that materials which are friable such as the carbonaceous chondrites would break down much more easily into dust size particles during asteroidal collisions, when compared with the meteorites with higher tensile strengths (Flynn, 2004). In the present case, it would be easier to conceive the collisional breakdown and release of metallic minerals from the more friable carbonaceous chondrites, rather than from iron or stony irons which have much higher tensile strengths. Therefore, a majority of the kamacites, taenites are possibly contributed by carbonaceous chondrites and some from ordinary chondrites, substantial contribution from iron or stony iron meteorites may be cautiously excluded.

The metal micrometeorites have been released due to comminution from their parent bodies in the asteroidal belt or from comets during their perihelion (comets are now known to contain kamacite particles : Brownlee, 2014) and have entered the Earth at low velocities and low entry angles to remain thermally unaltered. Also, the small particle sizes could have also played an important role in their survival without being thermally altered (Love and Brownlee, 1993).

Cooling Histories

Cooling rates of meteoritic taenites have been calculated using their sizes, based on variation in Ni contents from core to rim of the particles and diffusion rates by Wood (1967); Bevan and Axon (1980). Wood (1967) recognized that the nickel concentration profiles in taenites can be used to identify cooling histories of meteorites. The kamacites in the present study have differences in Ni contents within each of the particles to a tune of ~2-3% which is similar to those found in ordinary chondrites, and carbonaceous chondrites (Wood, 1967) (Table 1). The taenites show a wide variation in Ni contents in each of the particles (Table 1; Table 2 Supplement). This aspect is similar to those observed in ordinary chondrites (Afatalab and Wasson 1980; Rubin 1990). There are many taenites which show aqueous alteration. Some of these particles show greater variation (up to 30%) in nickel contents. We have measured nickel variation from rim to rim on four well preserved particles. Nickel diffusion in taenites shows distinct “M-shaped patterns” with increasing nickel contents towards the rims (Fig. 5), which are indicative of extremely slow cooling. We could calculate cooling rates for four well preserved taenites in this study, they range from $0.1^0 - >10^0\text{C/Ma}$ (Fig 6).. Based on similar calculations, the taenite in Toluca iron meteorite showed a cooling rate of $4^0 /$ million years (Wood, 1967). Bevan and Axon (1980) arrived at $1\text{K}/10^3$ years for taenites in Tieschitz H3 chondrite. It is important to note that the nickel variation in the taenites in this investigation suggests that their Ni contents are primary and have not been disturbed during atmospheric entry. In the phase diagram of cooling of Fe-Ni, at temperatures between $1430 - 700^0\text{C}$, taenite is the stable phase, whereas, at $\sim 700^0\text{C}$ kamacite begins to precipitate and is therefore stable at temperatures below 700^0C (Wood, 1967). This implies that even the largest of the kamacites measuring $\sim 400 \mu\text{m}$ has not reached temperatures in excess of $\sim 700^0 \text{C}$ during entry. Therefore all such particles must have affected a low entry angle, low velocity entry in order to have survived without undergoing thermal alteration.

This has significance in the present investigation, because atmospheric entry heating takes place for a few seconds followed by rapid cooling (Brownlee, 1985; Rudraswami et al. 2015). Nickel under such circumstances does not have sufficient time to diffuse and it remains uniform. This is found to be true for most of the Fe-Ni beads, but not for the kamacites and taenites. Slow diffusion and slow cooling rates confirms the taenites in this investigation as primary particles.

Origin of Fe-Ni beads

Among the collection, 50 particles are Fe-Ni beads that have homogeneous Ni contents (Fig. 2; Table 3,4). Homogeneous Ni contents in Fe-Ni beads is a common phenomenon in all the three

basic types (S-, G- and I-type) of cosmic spherules (Rudraswami et al. 2014b). The beads formed during atmospheric entry of carbonaceous chondritic precursors : During entry, due to pyrolysis of carbon contained in the incoming micrometeorites the particles experience an initial phase of reduction wherein the metal would tend to segregate as Fe-Ni beads which would be immiscible with the silicate matrix (Genge and Grady, 1998; Brownlee et al., 1984). The particles containing these beads would then be subjected heating and oxidation during which the immiscible beads would be separated due to density difference between the host and the bead and the beads would be released in the atmosphere. The size and Fe-Ni contents of these beads depend on the quantity of metal contained in the parent body and the heating and oxidation experienced during entry (Taylor et al. 2000; Rudraswami et al. 2014a; Cordier et al. 2011). The Fe-Ni beads could have been produced by several mechanisms. They have been traditionally found in I-type and G-type spherules (Blanchard et al., 1980; Finkelman 1970). Taylor et al (2000) reported 10% of the Antarctic S-type spherules to contain Fe-Ni beads. Rudraswami et al. (2014a) in an extensive investigation reported on 55 Fe-Ni beads in all the three basic types of cosmic spherules (I-type,G-type and the S-type) which had a size range of ~40 to >200µm with range of Ni contents from ~20% to >90%. The size range of beads observed by Rudraswami et al. (2014a) overlaps with the sizes of beads in the present investigation, so do the Fe, Ni and Co contents of the beads. All the beads observed by Rudraswami et al.(2014a) were suggested by them to have formed during atmospheric entry.

In addition, Fe-Ni beads with homogenous Fe-Ni contents can form due to shock heating of meteorites and have been reported from CM chondrites both in chondrules and from the matrix regions (Brearley and Jones, 1998; Kimura et al. 2011), therefore all homogeneous Fe-Ni beads need not be of secondary (i.e., formed during atmospheric entry) origin, but it is difficult to make such a distinction especially in the present collection. Metal phases in ordinary chondrites have a range of Fe-Ni compositions and have sizes up to few mm (Brearley and Jones, 1998), therefore it is not inconceivable that these metals gets dislodged during collisions and enter the atmosphere as alloys.

Therefore the following explanations seem plausible for the origin of the Fe-Ni beads :

1. Fe-Ni metal is a ubiquitous constituent of chondritic meteorites especially the ordinary chondrites (OC) which have 3- 20% of their constituents as metal (Jarosewich, 1990). It is conceivable that the metal from OC meteorites in the particulate forms could be released into the inner solar system during asteroidal collisions. The metal components have sizes up to several mm (Brearley and Jones, 1998). Any of such particles could have entered the atmosphere as Fe-Ni beads.

2. The beads are released from I-type spherules due to unequal heating leading to differential expansion – we observe several I-type spherules which have radial cracks emanating from the Fe-Ni portions up to the outer margins of spherules. This mechanism would eventually lead to the fragmentation and release of beads. Therefore the beads could be I-type spherules with their outer mantles removed.
3. The beads formed during atmospheric entry of carbonaceous chondritic precursors as observed in all the three basic types of cosmic spherules (the I-type, G-type and the S-type) and have been released during entry

Since the beads formed by all the above processes have highly overlapping Fe-Ni-Co contents it would not be easy to distinguish the parent sources for the beads in the present study.

Origin of I-type Spherules

Kamacite is the most common metal phase in all ordinary and most carbonaceous chondrites, followed by taenite and plessite (Smith et al., 1993; Rubin, 1988). This is the case in the present collection of unmelted metal as well. In meteorites, metal is more commonly present in the spherical form, rather than as metallic minerals (Rubin, 1994), because several conditions need to be satisfied for metal to develop into euhedral crystals, such as grain growth must occur at free surfaces, metallic Fe-Ni grains must remain undeformed during compaction, thermal metamorphism, aqueous alteration or shock (Rubin, 1994). The shapes of the particles (euhedral, sub-hedral or irregular) in this collection suggest that the grains have formed at free surfaces on their parent bodies or in the nebula.

The presence of a magnetite/wustite rim is a good criterion to show that unmelted micrometeorites entered the Earth's atmosphere as whole particles and are not fragments of bigger objects. Wustite commonly occurs in fusion crusts of iron meteorites and in most I-type cosmic spherules and has been simulated in artificial ablation experiments conducted under low oxygen fugacity (Blanchard and Davis, 1978) and it does not form under terrestrial conditions. The presence of wustite in the zoned rim on many particles (Figs 1c-f; Fig.3) suggests that rim development is an atmospheric entry phenomenon because wustite forms at high temperature and low oxygen fugacity, whereas magnetite can form under lower temperatures as well (Genge, 2016). While the presence of an oxidized rim is a good criterion to show that unmelted micrometeorites entered the Earth's atmosphere as whole particles however, the absence of rims can also mean that these particles were parts of larger meteorite fragments.

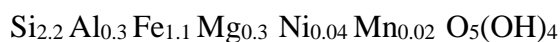
The I-type spherules are one of the three major types of cosmic spherules found commonly in all cosmic dust collections, they comprise a combination of magnetite and wustite. They have been suggested to have formed due to metal segregation in carbonaceous chondritic materials, subsequent release due to inertial forces followed by heating and oxidation of the released Fe-Ni beads during atmospheric entry (Blanchard et al. 1980; Brownlee et al. 1984). However, the presence of cosmogenic radionuclides in I-type spherules indicated that they were exposed to the space for substantial amounts of time, therefore they were suggested to be primary entities released due to collisions in their parent bodies and their elemental ratios suggested metal-rich carbonaceous chondritic bodies to be the precursors (Herzog et al. 1999). The observation of two phases of magnetite and wustite on the rims is a feature similar to the one observed in simulation experiments on iron meteorites, further heating would result in a texture which has magnetite and wustite interlocking crystals similar to those in I-type spherules (Blanchard and Davis, 1978). The size range of the metal micrometeorite particles also conforms to the sizes in which the I-type spherules have been reported in the literature (Prasad et al. 2013; Parashar et al. 2010; Taylor et al. 2000). Therefore, it is proposed here that the I-type spherules commonly found in all cosmic dust collections have multiple origins, and heating and oxidation of kamacites/taenites released from their parent bodies is an additional source. A similar suggestion has been given by Herzog et al. (1999), the present study confirms their hypothesis.

One issue that needs to be addressed, however, is that of the kamacite dimensions and those of the I-type spherules. The average sizes of the kamacites in the present study are around 50 μm or lower. After accounting for the degree of evaporative losses sustained by the I-type spherules, Herzog et al. (1999) assessed that the pre-atmospheric sizes of these particles fall in a size range of 300-400 μm . In contrast, Rubin and Wasson (1988) reveal that metal constitutes 20-40% of most chondrules, but it is in the form of spherules of 10-25 μm sizes and kamacite is the dominant phase. While it would be difficult to assume that the metal would be separated from the olivines in the chondrules and merge to form larger entities in the collisional processes, Herzog et al. (1999) also suggested an additional possibility of metal-rich chondrules of large diameters which can account for the average sizes of I-type spherules observed in the world collections. Prasad et al. (2013) analysed 26 I-type spherules in their collection which had an average diameter of $\sim 265 \mu\text{m}$, however their sample collection was biased towards the larger particles ($>200 \mu\text{m}$). All collections of melted micrometeorites suggest an average of 200 μm size for the particles (e.g., Taylor et al., 2000; Brownlee et al., 1997). Some of the kamacites in the present collection are quite large ($\sim 400 \mu\text{m}$, Fig. 1f; 6b) and there are others which are close to $\sim 300 \mu\text{m}$.

Aqueous Alteration and Planetological Implications :

Aqueous alteration is an important phenomenon in carbonaceous chondrites (Brearley, 2006). Majority of the investigators now believe that the appropriate P,T conditions, oxygen fugacity and more importantly water/rock ratio that facilitated aqueous alteration in meteorites can only be available on asteroidal parent bodies (Hanowski and Brearley, 2000). Kamacite is one of the most common minerals in all chondritic meteorites and is one of the first minerals to react with an ambient aqueous environment (Brearley, 2006). Aqueous alteration of kamacite leads to different end products which depend on the microchemical environment in which it undergoes the alteration process (Palmer and Lauretta, 2011) : In an environment that is sulfur-rich kamacite alters to the serpentine mineral tochilinite, whereas in the presence of Si and water the resultant product is cronstedtite. After the kamacite is deposited on the seafloor, the Fe-Ni reacts with H₂O and O₂ and forms Fe oxyhydroxides FeO (OH) which initially form as a coating on its surface. This surface has high adsorbing capacity because of the free charges present. It adsorbs all cations present in the environment (Mg, Si, Al etc.). With time there will be reconstitution of this unstable structure to a more stable one under these P-T conditions that forms a mineral phase. The alteration is indicated by the presence of hydrous phyllosilicate minerals. In meteorites, cronstedtite is a less common aqueously altered product when compared with tochilinite,. Sulfur is most common in all the meteorites. Aqueous alteration in the presence of sulphur leads to the formation of tochilinite. In an environment that contains sulfur, Tochilinite forms when the Fe released from the kamacitic phases reacts with the surrounding Si and Mg released during the aqueous alteration of pyroxenes and olivines (Tomeoka and Buseck, 1985). The oxygen isotopic ratios of the aqueously altered phases suggests that these reactions have taken place at temperatures <20⁰C (Clayton and Mayeda, 1984).

Almost all the particles show some signs of aqueous alteration due to their varying residence times on the deepsea floor, it is observed in a more pronounced manner in 29 particles which display different degrees of alteration (Fig.7a-f; Table 5). The Mg/Si/Fe ternary diagram (Fig. 8) has been used to identify various secondary phases of aqueous alteration of kamacite (McSween, 1987). Initially, additional Mg would result in Mg-rich cronstedtite, ultimately, the cronstedtite would absorb enough Si that it would become a ferroan serpentine (McSween, 1987; Tomeoka and Buseck, 1985). The aqueously altered particles in the present investigation show a systematic increase in Si, Mg and Al contents ranging from ~0.6-17.26% SiO₂; 0.2 – 7% MgO and 0.2 – 3.0% Al₂O₃ (Fig. 8; Table 5). The most altered portion of the particle (AAS 26-D9 M2-P7) in the present study has the following formula which conforms to that of a cronstedtite (Palmer and Lauretta, 2011):



Several hydrated particles appear to be approaching this composition (Table 5). The analytical totals are observed to decrease due to the addition of water into the structure, and particle dimensions increase with the absorption of water (Fig.7). Further alteration would have led to the transformation to a phase that would resemble poorly crystalline phase (PCP) found commonly in meteorites (Brearley and Jones, 1998).

Since the time of their fall, the particles would be interacting with the pore waters on the deep seafloor. Nath and Mudholkar (1989) analyzed the composition of pore waters from this part of the Indian Ocean. This area contains siliceous ooze sediments and the pore waters were extracted from the top ~40 cm of the sediment layer. The water overlying most of the deep-sea floor is saturated with oxygen or nearly so (5–6ml/litre). Based on the data presented by Nath and Mudholkar (1989), the kamacite particles are residing in an environment which has a pH of ~8 (alkaline and oxidizing environment), with high silica contents (~500 $\mu\text{g}_{\text{at}}/\text{l}$) in dissolved form, high because this is a siliceous ooze area.

The Fe in the kamacite, when it encounters the seafloor environment, would be oxidized to Fe^{+3} which reacts with the water leading to the formation of Fe oxyhydroxides. The elements Si, Al, Ca, K, Na are incorporated into this lattice and Ni is released into the ambient environment as it is not easily oxidized, it would remain in the suspended form or would be adsorbed onto the aqueously altered portion which shows the presence of Ni but in much reduced percentages. The cobalt in the kamacite also undergoes a similar fate as it does not oxidize easily.

The duration of the aqueous alteration is estimated as follows. The settling rate of a 100-200 μm particle in the deepsea is 10 m/day (Stemmann et al. 2004). For the average seafloor depth of 5200 m in the present study, each particle takes ~520 days to settle, traversing through a sea surface temperature of ~23 $^{\circ}\text{C}$ to 2 $^{\circ}\text{C}$, at the seafloor. There are particles which show no signs of aqueous alteration, which means that the particles do not alter visibly during their ~500-day transit to the seafloor. Apparently, significant alteration has taken place only after they were deposited on the seafloor. In addition, the collector dredge containing the magnetic assembly has a width of 70 cm which has the capability to penetrate the seafloor to a depth of 70 cm conforming to a maximum age of ~200,000 years (Parashar et al. 2010), however, it was designed to drag along the seafloor. Therefore, if we consider 15 cm as the average penetration, then the time of fall of the particles has an age range of ~1.5 – 50,000 years based on the sedimentation rates here (Prasad et al. 2013). It is

possible that several particles may have altered completely into serpentine clays much earlier than 50,000 years.

Lee and Bland (2004) investigated weathering of meteorites in Antarctica and hot deserts. Some of the changes observed in the meteoritic metal in Antarctic meteorites are similar to those observed here : increasing concentrations of Si, Mg and Ca and possible cronstedtite formation with increasing residence times. The metal in the Antarctic meteorites however did not show increase in their dimensions due to water absorption as shown by the kamacites in the deep seafloor (Fig 7). More importantly, the residence times of the meteorites they investigated ranged from 52-820 ky.

More recently, van Ginneken et al. (2016) observed 366 Antarctic micrometeorites for aqueous alteration. They found that metal in micrometeorites is invariably replaced by hydroxides accompanied by a reduction in the Ni/Fe ratios of the newly formed aqueously altered phases. Magnetite shows greater resistance to alteration when compared with Fe-Ni metal in micrometeorites. This result is similar to the present observation where the magnetite rims of the particles seem to be intact whereas, the Fe-Ni metal of kamacites seems to absorb water and expand beyond the original grain boundaries (Fig.7). The reduction in the Ni/Fe ratio however, has been attributed to the removal of Ni due to the circulation of slightly acidic antarctic water having low pH. The residence times of the studied micrometeorites was found to be close to 1 Ma (Suavet et al.2011). Therefore, apparently, the particles have taken extremely long residence times in order to develop the observed alteration features.

The particles in the present investigation show a range in aqueous alteration which is based on their residence times, chemical compositions (those with higher Fe contents, e.g., kamacites would alter more readily), and sizes. The particles in Antarctica are buried under water for close to a million years under reducing conditions as shown by the investigations of van Ginneken et al. (2016). The particles in the present investigation are buried under water (which is alkaline and is oxygenated) possibly up to 50,000 years. In both these cases, burial under water for long periods of time is common. It appears that there should be enough water to bury a small kamacite crystal for long periods of time in order for it to alter into a serpentine mineral under cold conditions. If we compound this to large meteorites containing aqueously altered kamacites, the implication could be that this meteorite (and parts of the parent body that contained this meteorite) was containing sufficient moisture over long periods of time.

Majority of investigators suggest that such continuous presence of water in the nebula may not have been a possibility, therefore the aqueous alterations observed in carbonaceous chondrites are suggested to have taken place in their parent bodies (Brearley, 2005).

The particles have been residing on the seafloor from ~1.5 to 50,000 years. They therefore present an opportunity to understand the long term behaviour of kamacites under aqueous conditions. Given this situation, they are the experimental equivalents of particles inserted in the deep sea environment for understanding long term exposure of kamacites to an alkaline environment. It is now understood that the Martian soil comprises of weathered products of basalt, salt, dust and also meteoritic material (Yen et al., 2005). Aqueous alteration minerals such as different types of salts indicate the quality of water in an environment. Therefore the search for life on Mars was also focused on aqueous alteration minerals (Boynton et al., 2009; Niles et al., 2013). Simulation experiments were carried out on kamacite because of its sensitivity as a tracer that can lead to the understanding of the quality of water (Berger, 2014). In this scenario, kamacites can be used as analogs to understand the aqueous alteration environment especially in the more alkaline regions of planetary surfaces such as the northern arctic plains of Mars. For example, the Phoenix Mars found the soils in the northern arctic plains of Mars to be alkaline with a pH of ~8-9 (Kounaves et al. 2010).

CONCLUSIONS

By raking the deep seafloor of the Indian Ocean with magnets fixed to a dredge, we recovered a variety of Fe-Ni rich particles that range from kamacites, plessites, taenites, and Fe-Ni beads. The Fe-Ni minerals have euhedral, subhedral or irregular shapes and have developed zoned oxidized rims due to heating and minimal oxidation during atmospheric entry and provide evidence for formation of I-type spherules from Fe-Ni minerals such as kamacites and taenites. They show extremely slow diffusion of nickel from the core to the rims indicating slow cooling at rates of $0.1^0 - >10^0$ C/ 10^6 yrs. Their euhedral/subhedral shapes further emphasize the fact that these are primary particles.

The Ni/Co ratios of the metallic minerals suggest that a majority of the particles could have originated from multiple parent meteorite sources, some of the kamacites and plessites however have Ni/Co ratios that fall in the zone of CM chondrites. Therefore, the Fe-Ni particles that rain on the Earth are sourced from multiple origins. This is in addition to their release as Fe-Ni beads from ablating meteoroids during atmospheric entry. There is also a possibility that some of the beads could be of primary origin.

Some of the particles have experienced aqueous alteration while resting on the seafloor, leading to the formation of the serpentine mineral cronstedtite. The seafloor provides a natural system for

understanding aqueous alteration of Fe-Ni minerals under cold, oxidizing conditions over a protracted amount of time. The finding of different forms of Fe-Ni minerals, Fe-Ni beads and high Ni particles adds to the known inventory of metal fluxes on the Earth.

Acknowledgments

The authors are grateful to CSIR-NIO for the facilities, Physical Research Lab for the sanction of the PLANEX project on micrometeorites. We express our gratitude to the Ministry of Earth Sciences, Govt. of India for funding of the project : “Surveys and Exploration for Polymetallic Nodules” during which the samples were collected. A.B. Valsangkar and S. Jaisankar are thanked for the immense help during sample collection. We are grateful to the reviewers G.F. Herzog and M.J. Genge for the incisive, detailed reviews which helped improve the manuscript considerably. We are indebted to D.E. Brownlee, the Associate Editor for helpful comments and suggestions that helped in improving the manuscript further.

This is NIO's contribution number XXXXXX

REFERENCES

- Afiatalab F. and Wasson J.T. 1980. Composition of the metal phases in ordinary chondrites: implications regarding classification and metamorphism. *Geochimica et Cosmochimica Acta* 44: 431–446.
- Badjukov D. D., Brandstaetter F., Raitala J., and Kurat G. 2009. Unmelted FeNi metal micrometeorites from the Novaya Zemlya glacier. *Lunar Planetary Science Conference* 40:1499 (abs).
- Berger, G. 2014. Alteration of meteorite-derived kamacite in martian regolith: A new insight of chemical processes in martian soils. *International Conference on Mars VIII: 1212*.
- Bevan, A. W. R., and Axon H.J. 1980. Metallography and thermal history of the Tieschtz unequilibrated meteorite – Metallic chondrules and the origin of polycrystalline taenite. *Earth and Planetary Science Letters* 47 : 353-360
- Bibring, J.P., Langevin Y., Poulet F., Gendrin A., Gondet B., Berthé M., Soufflot A., Drossart P., Combes M., Bellucci G., Moroz V., Mangold N., Schmitt B, and the OMEGA team 2004. Perennial water ice identified in the south polar cap of Mars. *Nature* 428: 627-630.
- Blanchard M.B. 1972. Artificial meteor ablation studies : iron oxides . *Journal of Geophysical Research* 77, 2442-2455.
- Blanchard M.B., and Davis A.S. 1978. Analysis of ablation debris from natural and artificial iron meteorites. *Journal of Geophysical Research* 83:1793-1808.
- Blanchard, M. B., Brownlee D.E., Bunch T.E., Hodge P.W., and Kyte F.T. 1980. Meteoroid ablation spheres from deep sea sediments. *Earth and Planetary Science Letters* 46:178–190.

Boynnton, W.V., Ming D.W., Kounaves S.P., Young S.M.M., Arvidson R.E., Hecht M.M., Hoffman J., Niles P.B., Hamara D.K., Quinn R.C., Smith P.H., Sutter B., Catling D.C., and Morris R.V. 2009. Evidence for calcium carbonate at the Mars Phoenix landing site. *Science* 325 : 61-64

Brearley A. J. 2005. Nebular versus parent body processing, in *Meteorites, Comets, and Planets*, edited by A.M. Davis, pp247-268, Elsevier.

Brearley A. 2006. In: *Meteorites and the Early Solar System II*, ed. by D. Lauretta and H. McSween, U. of Ariz. Press, Tucson, 587-624

Brearley, A. J., and Jones R.H. 1998. Chondritic meteorites. In *Planetary materials*, edited by Papike J. J. *Reviews in Mineralogy*, vol 36. pp. 1–398 Washington, D.C.: Mineralogical Society of America.

Brownlee D. E. 1985 Cosmic dust: Collection and research, *Annual Reviews Earth and Planetary Science* 13: 147–173.

Brownlee D.E. 1981. Extraterrestrial components. In *The Sea*, vol. 7 edited by E. Emiliani, Wiley, New York., p. 733-762.

Brownlee D. E. 2014. The Stardust Mission: Analyzing Samples from the Edge of the Solar System, *Annual Reviews Earth and Planetary Science*, 42:179–205.

Brownlee D.E., and Hodge P.W. (1973) Ablation debris and primary micrometeoroids in the stratosphere. In *COSPAR SPACE RESEARCH XIII*, edited by Rycroft M.J. and S.K. Runcorn, Akademie, Verlag, Berlin, pp 1139-1151

Brownlee D. E., Bates B., and Beauchamp R. H. 1983. Meteor ablation spherules as chondrule analogs. In *Chondrules and their origin*, edited by King E. A. Houston, Texas: Lunar and Planetary Institute. pp. 10–25.

Brownlee D. E., Bates B. A., and Wheelock M. M. 1984. Extraterrestrial platinum group nuggets in deep-sea sediments. *Nature* 309:693–695.

Brownlee D. E., Bates B., and Schramm L. 1997. The elemental composition of stony cosmic spherules. *Meteoritics & Planetary Science* 32:157–175.

Ciesla F. J., Lauretta D.S., Cohen B.A., and Hood L.L. 2003., A Nebular Origin for Chondritic Fine-Grained Phyllosilicates. *Science* 299: 549-552.

Clayton, R. N., and Mayeda T.K. 1984., The oxygen isotope record in Murchison and other carbonaceous chondrites, *Earth and Planetary Science Letters* 67: 151-161.

Cordier C., van Ginneken M., and Folco L. 2011. Nickel abundance in stony cosmic spherules: Constraining precursor material and formation mechanisms. *Meteoritics and Planetary Science* 46 : 1110-1132.

Flynn G.J. 2004. Physical properties of meteorites and interplanetary dust particles :clues to the properties of the meteteors and their parent bodies. *Earth Moon and Planets* 95 : 361–374.

Folco L. and Cordier C. 2015. Micrometeorites. In *European Mineralogy Union Notes in Planetary Mineralogy*, 15 : 253-297. DOI : 10.1180/EMU – Notes 15.9

- Genge M.J. 2006. Igneous rims on micrometeorites. *Geochimica et Cosmochimica Acta* 70: 2603-2621.
- Genge M.J. 2016. The origins of I-type spherules and the atmospheric entry of iron micrometeoroids. *Meteoritics and Planetary Science* 51:1063-1081
- Genge M.J., Engrand C., Gounelle M. and Taylor S. 2008. The classification of micrometeorites. *Meteoritics and Planetary Science* 43 : 497-515
- Genge, M. J. and Grady M.M. 1997. The fusion crusts of carbonaceous chondrites: Implications for melted micrometeorites, *Meteoritics and Planetary Science* 32 : A45_A46.
- Genge, M. J., and Grady M.M. 1998., Melted micrometeorites from Antarctic ice with evidence for the separation of immiscible Fe-Ni-S liquids during entry heating, *Meteoritics and Planetary Science* 33 : 425–434.
- Goldstein J.I., Yang J., and Scott E.R.D. 2014. Determining cooling rates of iron and stony-iron meteorites from measurements of Ni and Co at kamacite–taenite interfaces. *Geochimica et Cosmochimica Acta* 140: 297–320
- Grossman L. and Larimer J.W. (1974), Early chemical history of the solar system, *Reviews in Geophysics* 12 : 71–101.
- Hanowski, N.P., and Brearley A.J. 2000. Iron-rich aureoles in the CM carbonaceous chondrites, Murray and Murchisson and ALH81002: Evidence for insitu alteration, *Meteoritics and Planetary Science* 35 :1291–1308.
- Herzog, G. F., Xue S., Hall G.S., Nyquist L.E., Shih C.Y., Wiesmann H., and Brownlee D.E.1999. Isotopic and elemental composition of iron, nickel, and chromium in type I deep-sea spherules: Implications for origin and composition of the parent micrometeoroids. *Geochimica et Cosmochimica Acta* 63 : 1443–1457.
- Hua X., Eisenhour D.D., and Buseck P.R. 1995. Cobalt-rich nickel poor metal (wairauite) in the Ningqiang carbonaceous chondrite. *Meteoritics* 30: 106-109.
- Jarosewich E. 1990. Chemical analyses of meteorites: A compilation of stony and iron meteorite analyses. *Meteoritics* 25:323–337.
- Kerridge, J. F., and Bunch T.E. 1979. Aqueous alteration on asteroids: Evidence from carbonaceous meteorites. In *Asteroids*, ed. T. Gerhels, pp. 610-611, The University of Arizona Press, Tucson & London.
- Kimura M., Grossman J.N., and Weisberg M.K. 2008., Fe-Ni metal in primitive chondrites - Indicators of classification and metamorphic conditions for ordinary and CO chondrites. *Meteoritics and Planetary Science* 43 : 1161-1171.
- Kimura M., Grossman J.N., and Weisberg M.K. 2011. Fe-Ni metal and sulfide minerals in CM chondrites: An indicator for thermal history. *Meteoritics and Planetary Science* 46 : 431–442.
- Kounaves S.P., Stroble S.T., Anderson R.M., Moore Q., Catling D.C., Douglas S., McKay C.P., Ming D.W., Smith P.H., Tamppari L.K., and Zent A.P.. Discovery of natural perchlorate in the

- Antarctic Dry Valleys and its global implications. *Environmental Science and Technology* 44:2360-2364.
- Kurat, G., Koeberl C., Presper T., Brandstatter F., and Maurette M. 1994. Petrology and geochemistry of Antarctic micrometeorites, *Geochimica et Cosmochimica Acta* 58 : 3879–3904.
- Lee M.R. and Bland P.A. 2004. Mechanisms of weathering of meteorites recovered from hot and cold deserts and the formation of phyllosilicates. *Geochimica et Cosmochimica* 68: 893–916,
- Love S. G. and Brownlee D.E. 1993. A direct measurement of the terrestrial mass accretion rate of cosmic dust. *Science* 256: 550–553.
- Maurette, M., Jéhanno C., Robin E., and Hammer C. 1987. Characteristics and mass distribution of extraterrestrial dust from the Greenland ice cap. *Nature* 328 : 699–702.
- McSween H. Y. Jr. 1987. Aqueous alteration in carbonaceous chondrites—Mass balance constraints on matrix mineralogy. *Geochimica et Cosmochimica Acta* 51: 2469–2477.
- Nath B. N., and Mudholkar A.V. 1989. Early diagenetic processes affecting nutrients in the Central Indian Ocean cores. *Marine Geology* 86 : 57-65.
- Niles P. B., Catling D. C., Berger G., Chassefière E., Ehlmann B.L., Michalski J. R., Morris R. V., Ruff S. W. and Sutter B.(2013) Geochemistry of carbonates on Mars: implications for climate history and nature of aqueous environments. *Space Science Reviews* :174, 301–328
- Palmer E. E., and Lauretta D.S. 2011. Aqueous alteration of kamacite in CM chondrites, *Meteoritics and Planetary Science* 46 : 1587-1607.
- Parashar K., Shyam Prasad M., and Chauhan S. S. 2010. Investigations on a large collection of cosmic dust from the Central Indian Ocean. *Earth, Moon, and Planets* 107 : 197–217.
- Plane J. M. C. 2012. Cosmic dust in the Earth’s atmosphere, *Chemical Society Reviews* 41: 6507–6518.
- Pouchou J. L., and Pichoir F. 1991. Quantitative analysis of homogeneous or stratified microvolumes applying the model “PAP” In *Electron probe quantification*, edited by K. F. J. Heinrich and D. E. Newbury, pp. 31–75, New York: Plenum Press.
- Prasad M. S., Rudraswami N.G., and Panda D.K. 2013. Micrometeorite flux on Earth during the last ~50,000 years. *Journal of Geophysical Research* 118 : 2381–2399.
- Rambaldi E. R. 1976. Trace element content of metals from L-group chondrites, *Earth and Planetary Science Letters* 31 : 224-238.
- Rambaldi E. R. 1977. Trace element content of metals from H- and LL-group chondrites, *Earth and Planetary Science Letters* 36 : 347-358.
- Robin E., Jéhanno C., and Maurette M. 1988. Characteristics and origin of Greenland FeNi cosmic grains, *Proc. Lunar Planetary Science Conference XVIII* : 593–598.
- Rochette P., Folco L., d’Orazio M., Suavet C., and Gattacceca J. 2009. Large iron spherules from the Transantarctic mountains : where is the nickel? *METSOC* 72 : 5097 (abs).

- Rubin A. E. 1988. Kamacite in ordinary chondrites (abstr.). *Meteoritics* 23 : 299.
- Rubin A. E. 1990. Kamacite and olivine in ordinary chondrites: Intergroup and intragroup relationships *Geochimica et Cosmochimica Acta* 54 : 1217–1232.
- Rubin A.E. 1994. Euhedral tetrataenite in the Jelica meteorite. *Mineralogical Magazine* 58 : 215–221.
- Rudraswami N. G., Prasad M.S., Plane J.M.C., Berg T., Feng W., and Balgar S. 2014a. Refractory metal nuggets in different types of cosmic spherules, *Geochimica et Cosmochimica Acta* 131 : 247–266.
- Rudraswami N. G., Prasad M.S., Babu E.V.S.S.K. and Vijaya Kumar T. 2014b. Chemistry and petrology of Fe–Ni beads from different types of cosmic spherules: Implication for precursors, *Geochimica et Cosmochimica Acta*, 145:139-158.
- Rudraswami N.G., Prasad M.S., Dey S., Plane J.M.C., Feng W. and Taylor S.2015. Evaluating changes in the elemental composition of micrometeorites during entry into the Earth's atmosphere. *The Astrophysical Journal* 814 : 78 (11pp) doi:10.1088/0004-637X/814/1/78.
- Sepp B., Bischoff A., and Bosbach D. 2001. Low temperature phase decomposition in iron-nickel of the Portales Valley meteorite, *Meteoritics and Planetary Science* 36 :587-595.
- Smith D. G. W., and Launspach S.1991. The composition of metal phases in Bruderheim (L6) and implications for the thermal histories of ordinary chondrites – Erratum, *Earth and Planetary Science Letters* 102 : 79-93.
- Smith D. G. W., Miura Y., and Launspach S. 1993. Fe, Ni and Co variations in the metals of some antarctic chondrites, *Earth and Planetary Science Letters* 120 : 487-498.
- Stemmann L., G Jackson G.A., and Gorsky G. 2004. A vertical model of particle size distributions and fluxes in the midwater column that includes biological and physical processes—part II: Application to a three-year survey in the NW Mediterranean Sea. *Deep-Sea Research I* 51 : 885–908.
- Suavet C., Rochette P., Kars M., Gattacceca J. , Folco L., and Harvey R.P. 2009. Statistical properties of the Transantarctic Mountains (TAM) micrometeorite collection. *Polar Science*. 3 :100–109.
- Suavet C., Gattacceca J., Rochette P. and Folco L. 2011. Constraining the terrestrial age of micrometeorites using their record of the Earth's magnetic field polarity. *Geology* 39 : 123–126.
- Tagle R., and Berlin J. 2008., A database of chondrite analyses including platinum group elements, Ni, Co, Au, and Cr: Implications for the identification of chondritic projectiles. *Meteoritics and Planetary Science* 43 : 541–559.
- Taylor S., Lever J.H. and Harvey R.P. 2000. Numbers, types, and compositions of an unbiased collection of cosmic spherules. *Meteoritics and Planetary Science* 35:651-666.

Tomeoka K., and Buseck P. R. 1985., Indicators of aqueous alteration in CM carbonaceous chondrites: Microtextures of a layered mineral containing Fe, S, O and Ni, *Geochimica et Cosmochimica Acta* 49 : 2149-2163.

Van Ginneken, M., Folco L., Cordier C., and Rochette P. (2012), Chondritic micrometeorites from the Transantarctic Mountains. *Meteoritica and Planetary Science* 47 : 228–247.

Van Ginneken M., Genge M.J. , Folco L. , and Harvey R.P. 2016. The weathering of micrometeorites from the Transantarctic Mountains. *Geochimica et Cosmochimica Acta* 179 : 1–31

Wood, J. A.1967. Chondrites: Their metallic minerals, thermal histories, and parent planets. *Icarus* 6: 1-49.

Yen A.S., Gellert R., Schroder C., Morris R.V. , Bell K.F., Knudson A.T., Clark B.C., Ming D.W., Crisp J.A., Arvidson R.E., Blaney D., Bruckner J., Christensen P. R., DesMarais D.J., de Souza P. A., Economou T. E., Ghosh A., Hahn B. C., Herkenhoff K. E., Haskin L. A., Hurowitz J. A., Joliff B. L., Johnson J. R., Klingelhofer G., Madsen M. B., McLennan S.M., McSween H. Y., Richter L., Rieder R., Rodionov D., Soderblom L., Squyres S. W., Tosca N. J., Wang A., Wyatt M. and Zipfel J. (2005) An integrated view of the chemistry and mineralogy of martian soils. *Nature* :436, , 49–54

FIGURE LEGENDS

FIGURE 1 :

Backscattered SEM images of unmelted metal-rich cosmic grains.

a: Taenite grain without a rim (Ni=35%)

b: Euhedral taenite with a thin oxidized rim.

c: Sub-hedral kamacite with a thick oxidized rim.

d: The oxidized rim in “c” under higher magnification showing an outer, darker magnetite and an inner wustite.

e: A kamacite grain enclosing a taenite inclusion, the grain is surrounded by a thin oxide rim.

f: Euhedral plessite (Ni=18%) showing a thin oxide rim and also the effects of post-depositional aqueous alteration (earthy portions).

g: Large sized (294 μm) Fe-Ni bead with a zoned rim.

h : Zoned rim in “e” under higher magnification. An outer dark magnetite and an inner wustite is seen with distinct differences in Ni contents. Apparently, the rim has developed during atmospheric entry due to minimal heating and oxidation, continuation of this process could lead to the formation of an I-type spherule.

FIGURE 2 : Backscattered SEM images of Fe-Ni beads.

a, b, c are unoxidized beads; d,e,f are oxidized beads. The oxidized beads contain numerous cracks which could have formed due to oxidation of Fe. The corresponding chemical compositions of the unoxidized and oxidized beads are presented in Tables 3 and 4 respectively.

FIGURE 3 : Backscattered SEM images showing a sequence of formation of I-type spherules with increasing heating and oxidation during atmospheric entry. (a) Fe-Ni bead without an oxide layer (b) Bead which has undergone minimum heating during entry leading to the formation of a wustite rim. (c-e) Fe-Ni bead with progressive heating and oxidation shows wustite and magnetite formation and development into interlocking crystals and the reduction in the size of the bead (f) The formation of a platinum group nugget after complete heating and oxidation of the bead. The unoxidisable noble elements within the spherule segregate into a Pt-group nugget (Brownlee et al., 1984).

FIGURE 4 : Ni/Co plots of kamacites, plessites and taenites in the present study. The kamacites in the bottom left part of the figure seem to fall in overlapping zones of CM, CV, CO and Ordinary Chondrites, however, a substantial number of kamacites and plessite occur in CM chondrites zone. Some of the taenites which are enriched in cobalt seem to fall around the zone defined for ordinary chondrites. The cobalt poor taenites fall in overlapping zones between iron, stony meteorites and CO chondrites. CO chondritic data from Kimura et al. (2008), CM chondritic data from Kimura et al. (2011), ordinary chondrite data from Rambaldi (1976; 1977); Rubin (1990); Afatalab and Wasson (1979), and Smith et al. (1991; 1993), Iron and stony meteorite data from Goldstein et.al. (2014).

FIGURE 5 : Diffusion plots of Ni distribution in taenites and plessites. Typical M-shaped diffusion plots are indicative of slow cooling.

FIGURE 6 : Cooling rates of nickel in taenites plotted as per the Wood (1967) model. The particles show cooling rates that range from 0.1^0 - $>10^0$ C/million years.

FIGURE 7 : Backscattered SEM images of cosmic metal grains which have suffered aqueous alteration..

a: The beginning of hydration and aqueous alteration with development of grooves from the rim of the particle.

b: The largest kamacite in the present collection, showing euhedral shape and aqueous alteration in a more advanced state.

c & d : The shapes of minerals are distorted, and they have expanded in size with the absorption of water and other elements. The oxidized rims of the particles developed during entry are discernible.

Further alteration would lead to the formation of particles that would resemble poorly crystalline particles (PCPs) found in carbonaceous chondrites (Brearley and Jones, 1998).

e: Fe-Ni bead with an oxidized rim showing extremes of aqueous alteration on the edges. The existence of a rim is also proof that this Fe-Ni bead was released during entry and has developed a zoned rim due to minimal heating during entry. The aqueous alteration has taken place during its residence time on the oceanfloor.

f: Extreme aqueous alteration to fibrous clay on the edges of the Fe-Ni bead shown in (e).

In all the above cases, magnetite rim appears to be more resistant to aqueous alteration than the Fe-Ni portions.

FIGURE 8 : Ternary diagram (after Tomeoka and Buseck, 1985) showing progressive aqueous alteration of kamacites/taenites in the present study from a start point of a kamacite, the alteration leads to their plotting on the Tohilinite Cronstedtite Intersection (TCI) line and approaching a composition that is closer to cronstedtite.

Fig. 1

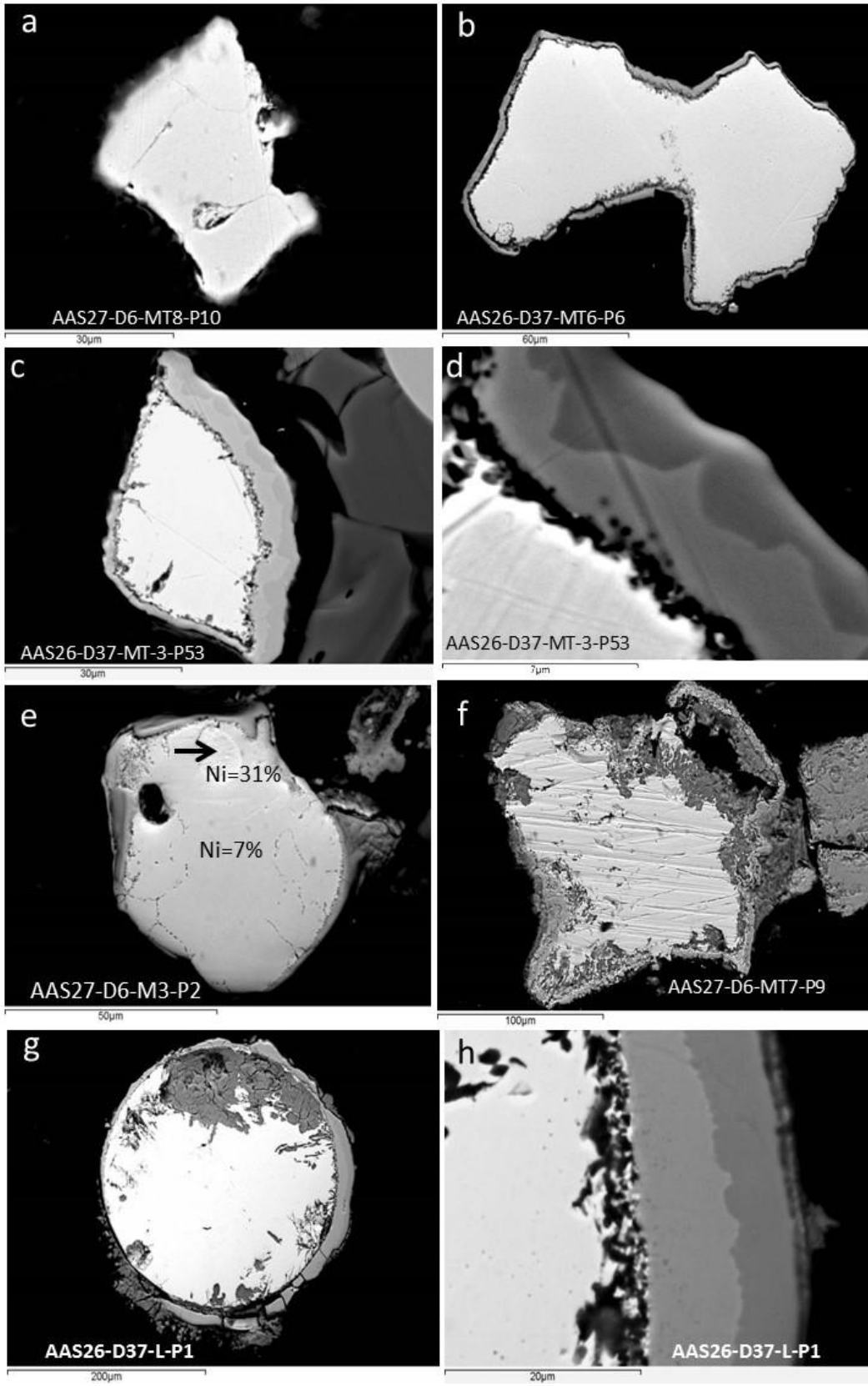


Fig. 2

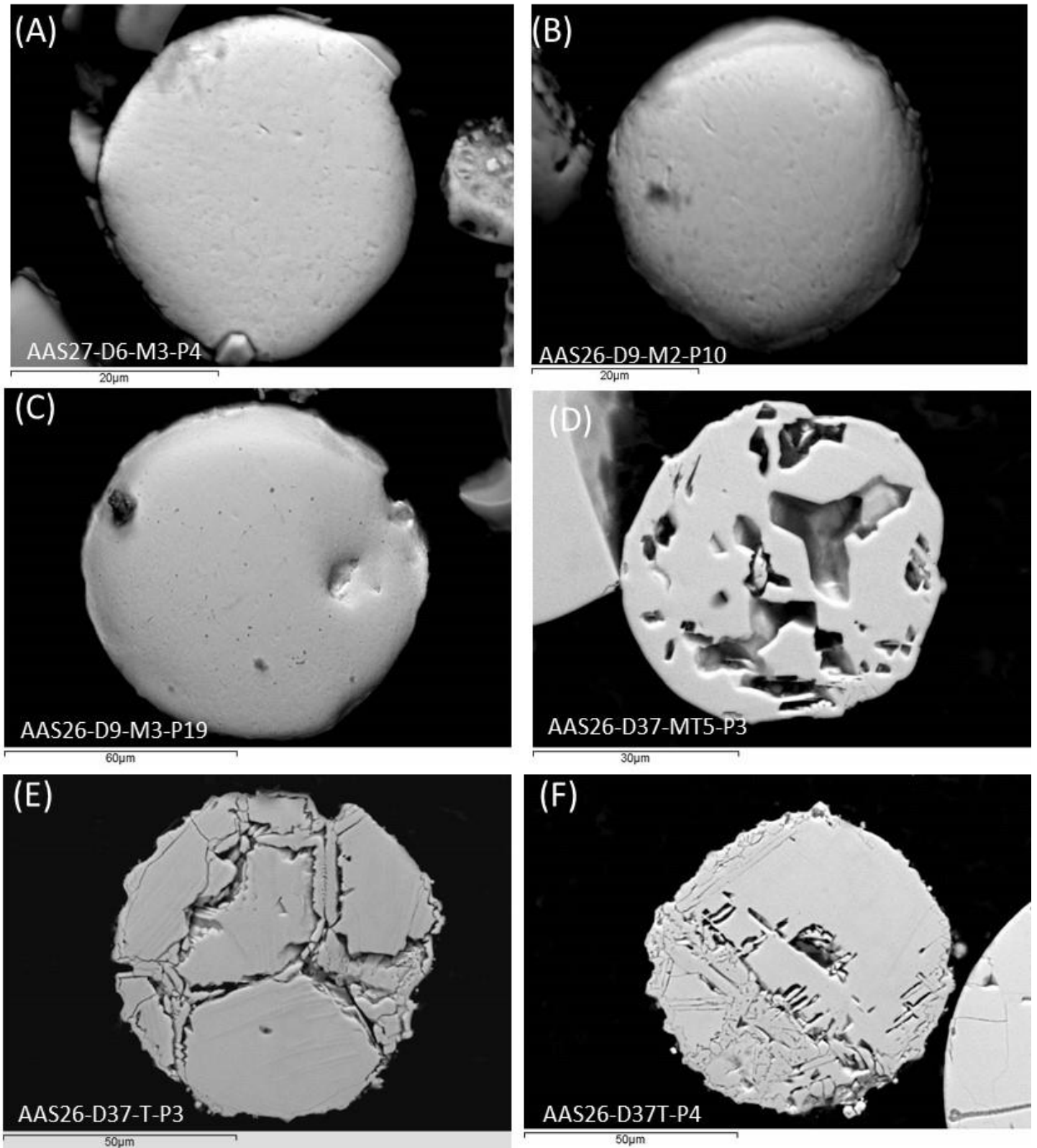


Fig. 3

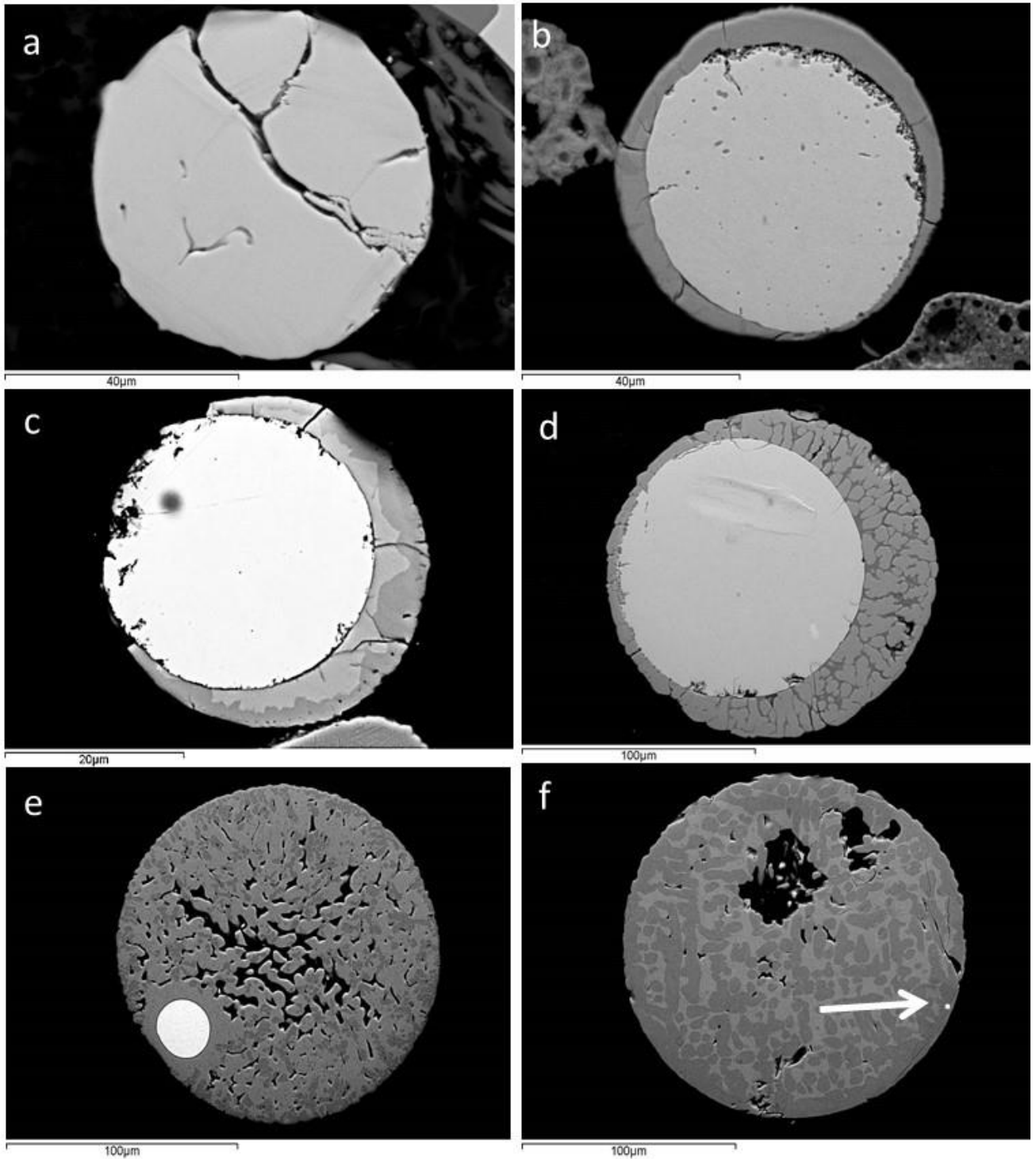


Fig. 4

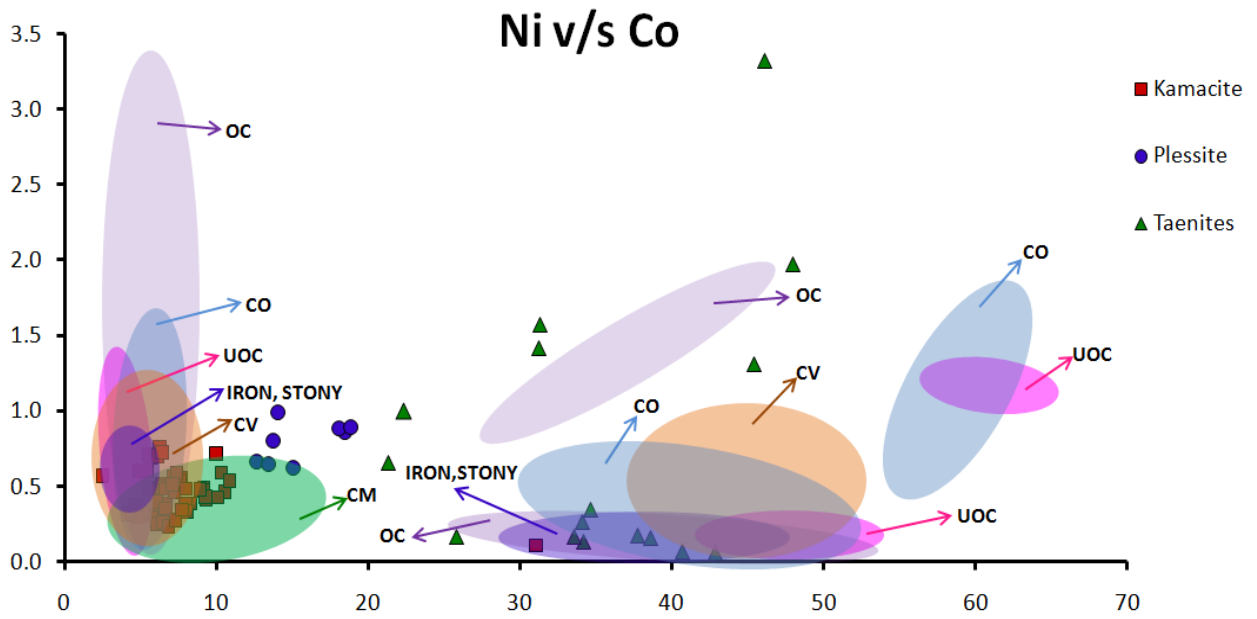
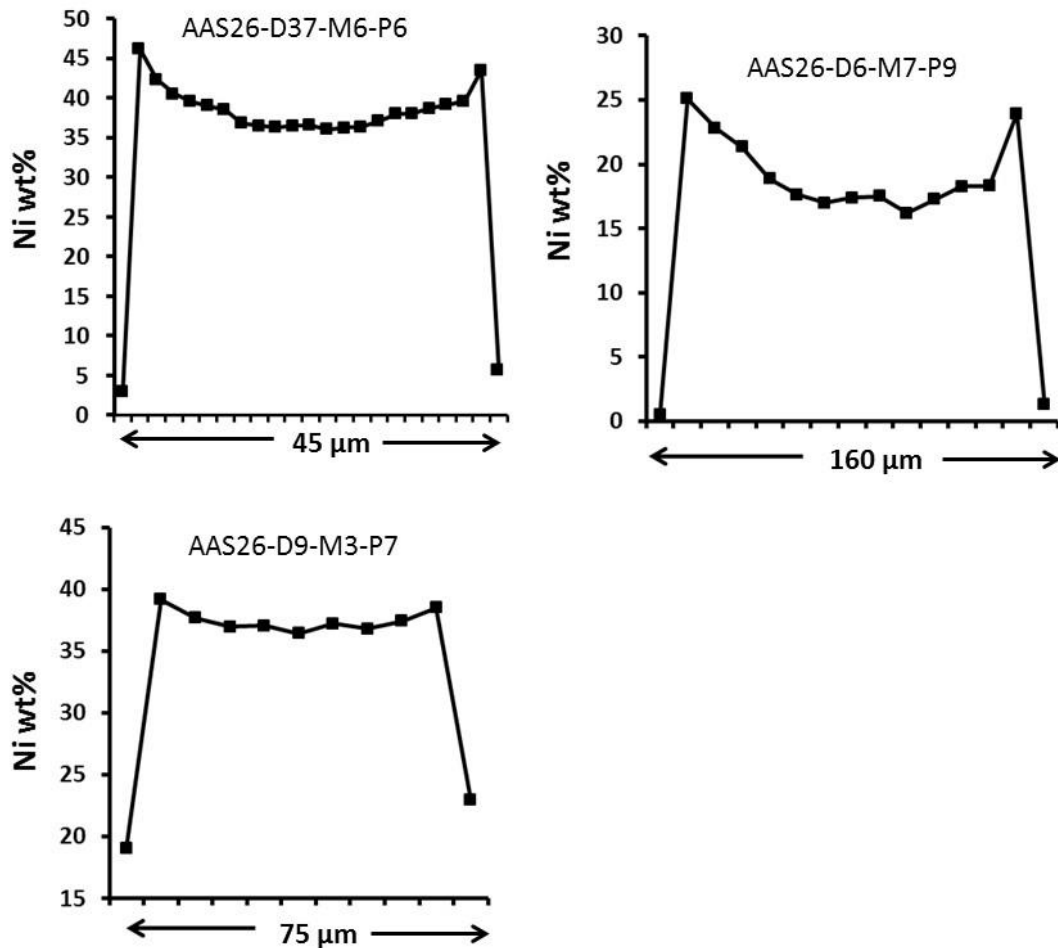


Fig. 5



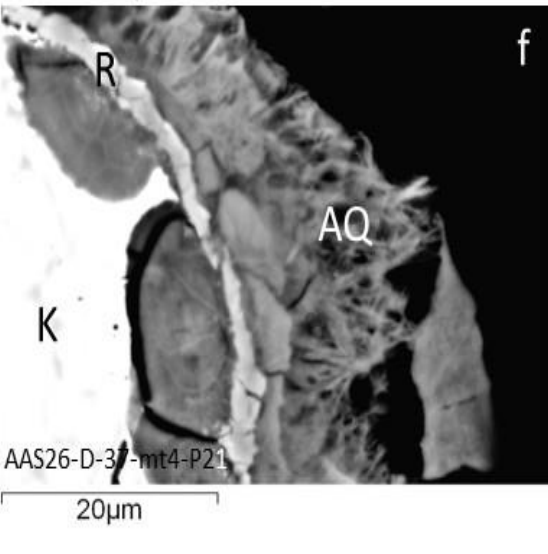
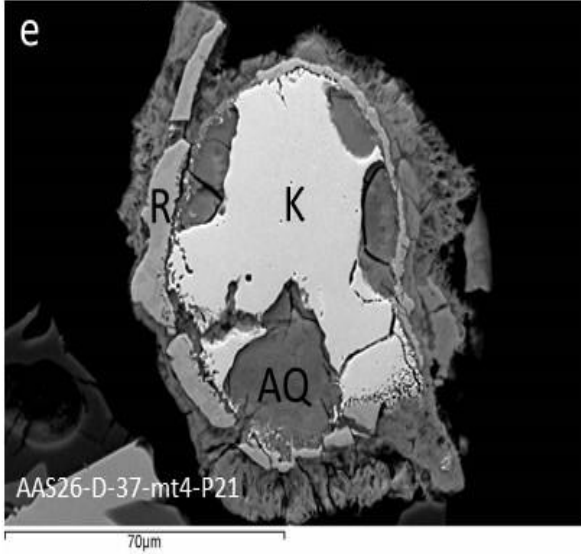
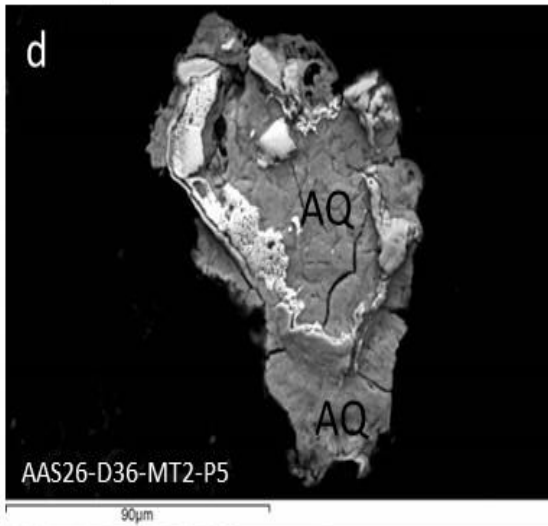
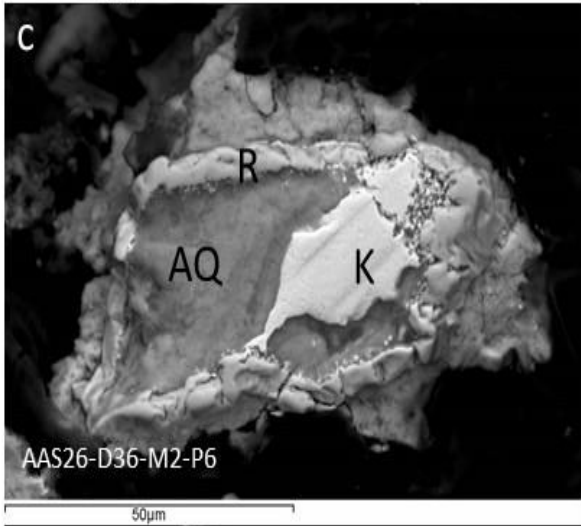
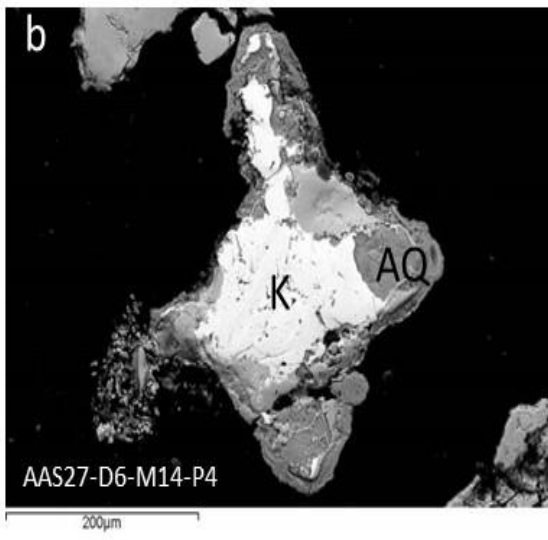
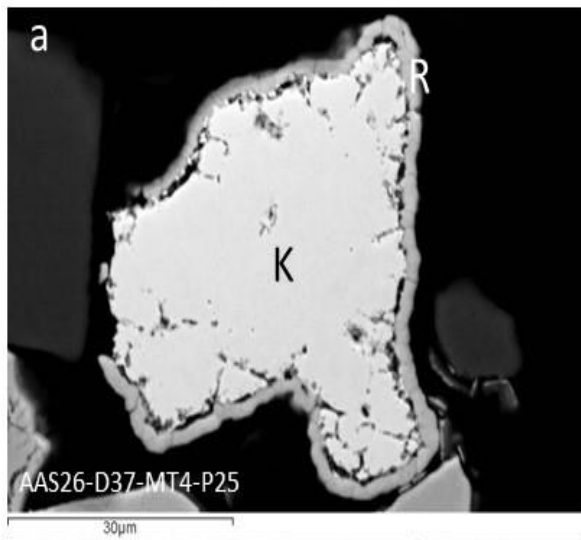


Fig. 6

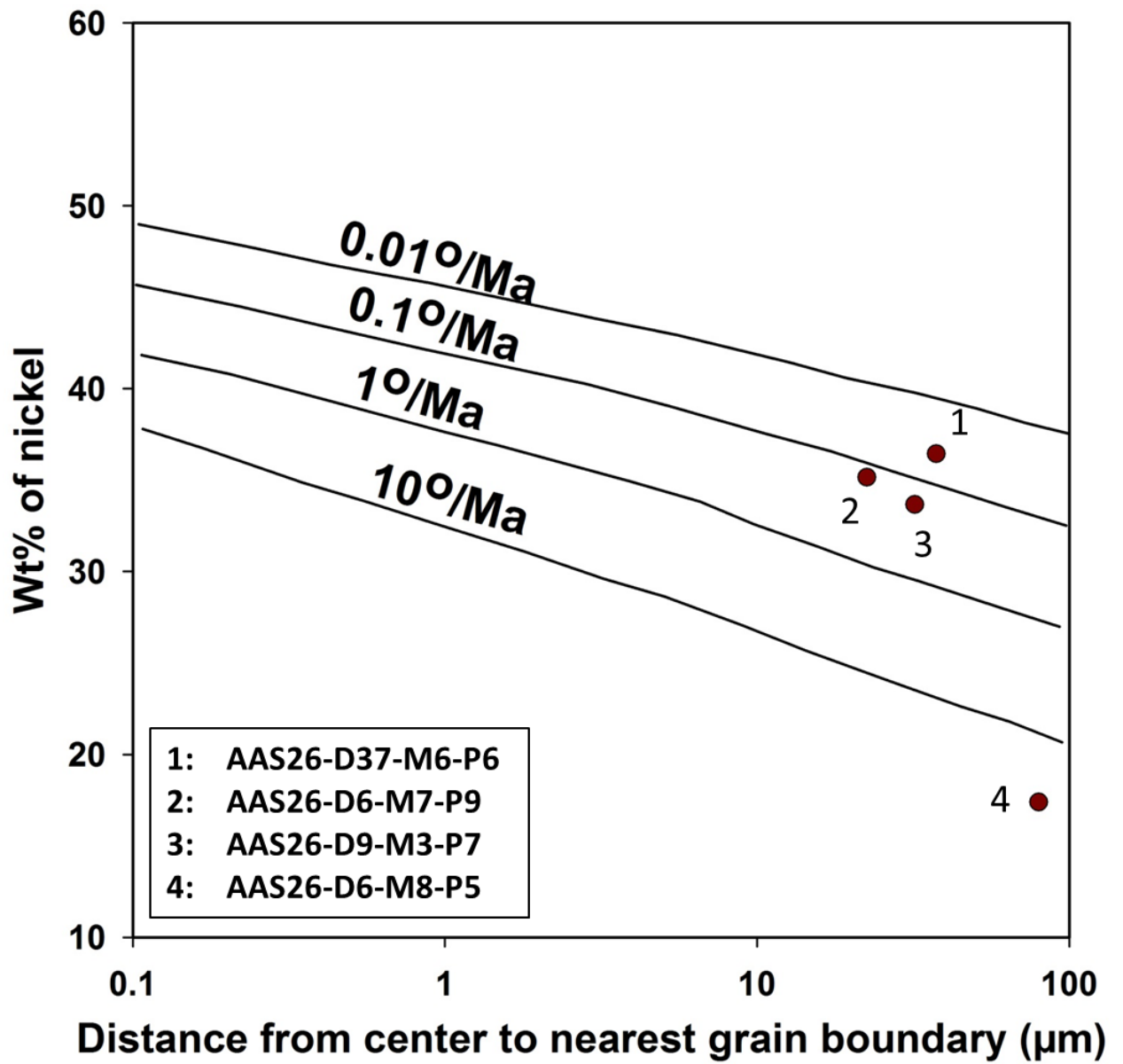


Fig. 7

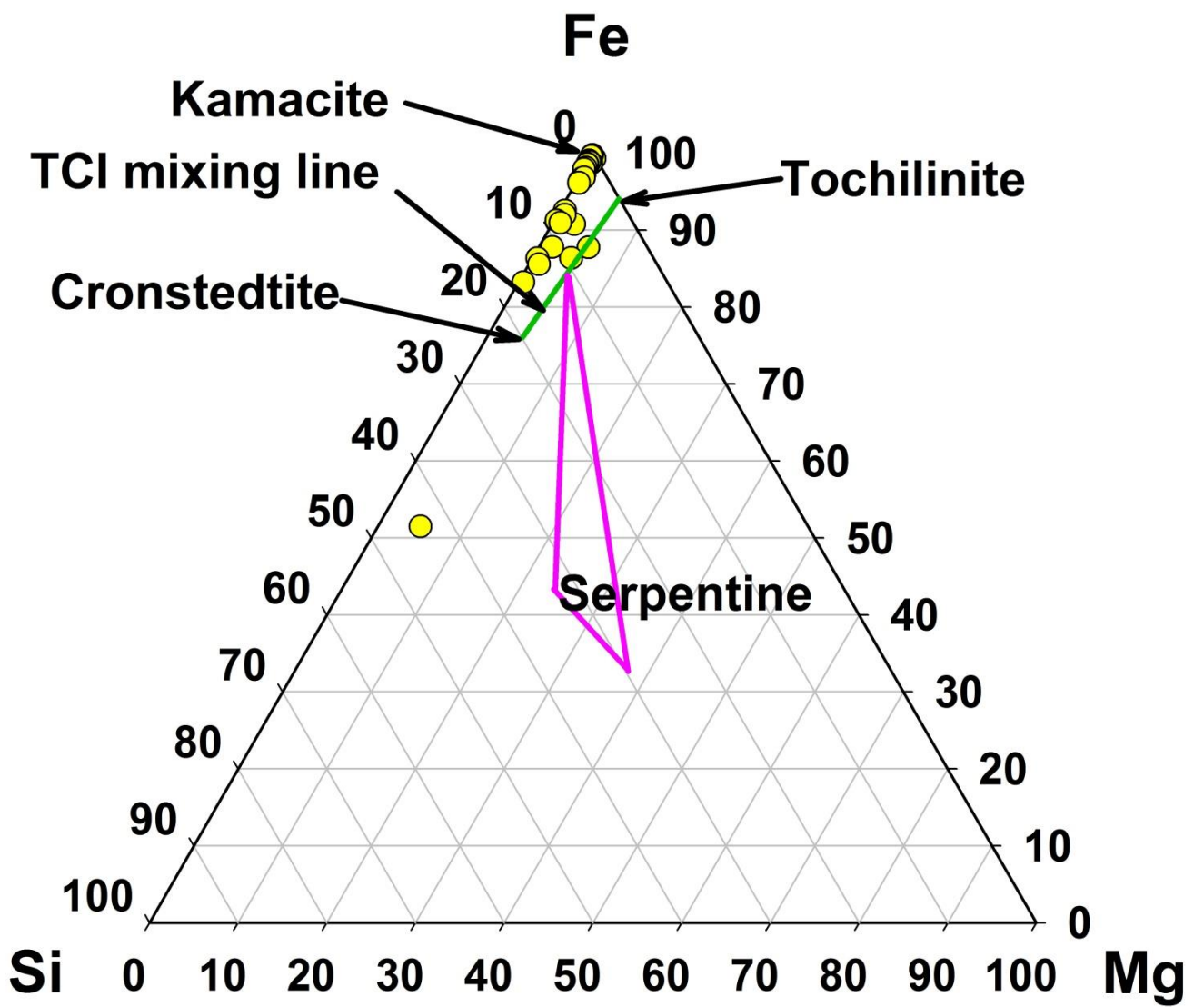


Fig. 8

TABLE 1 : Chemical composition of kamacites, plessites and taenites

S. No.	SAMPLE No and TYPE	Size μm	no of pts analyzed	Fe (2 σ)	Co (2 σ)	Ni (2 σ)	TOTAL
1	AAS26-D37 M1-P13 KAMACITE	142x68	7	89.3 (1.8)	0.3 (0.1)	5.5 (0.24)	95.0
2	AAS26-D37M1-P15 KAMACITE	60x35	13	89.7 (1.74)	0.4 (0.06)	5.9 (0.66)	95.9
3	AAS26-D37-M2-P6 KAMACITE	83x67	8	91.3 (1.8)	0.6 (0.1)	5.2 (1.3)	97.1
4	AAS26-D37-M2-P13 KAMACITE	21x25	2	86.4 (1)	0.4 (0.04)	8.9 (0.1)	95.7
5	AAS26-D37-M3-P2 KAMACITE	119x64	2	85.5 (2.9)	0.4 (0.02)	7.7 (0.8)	93.6
6	AAS26-D37-M3-P23 KAMACITE	196x105	2	82.7 (0.6)	0.5 (0.1)	8.4 (0.1)	91.5
7	AAS26-D37-M3-P29 KAMACITE	125x96	3	91.4 (2.3)	0.4 (0.06)	6.5 (0.3)	98.3
8	AAS26-D37-M3-P53 KAMACITE	35x52	10	93.6 (1.9)	0.6 (0.1)	4.9 (0.4)	99.1
9	AAS26-D37-M4-P17 KAMACITE	27x42	4	87.3 (2.2)	0.5 (0.02)	10.3 (0.1)	98.1
10	AAS26-D37-M4-P20 KAMACITE	58x30	4	84.9 (2)	0.6 (0.04)	5.2 (0.4)	90.8
11	AAS26-D37-M4-P21 KAMACITE	116	3	89.8 (1.6)	0.3 (0.1)	4.6 (0.2)	94.7
12	AAS26-D37-M4-P25 KAMACITE	50x44	9	84.4 (2.3)	0.3 (0.1)	4.6 (0.2)	89.3
13	AAS26-D37-M5-P4 KAMACITE	108x142	5	89.2 (0.6)	0.4 (0.06)	7.8 (0.4)	97.4
14	AAS26-D37-M6-P12 KAMACITE	35x43	5	89.6 (3.1)	0.6 (0.1)	6.9 (0.16)	97.1
15	AAS26-D36-M1-P2 KAMACITE	57x50	11	89.5 (1.7)	0.5 (0.1)	5.2 (0.2)	95.2
16	AAS26-D36-M2-P6 KAMACITE	86x66	6	94.2 (2.3)	0.3 (0.1)	4.7 (0.1)	99.3
17	AAS26-D36-M5-P4 KAMACITE	38x32	6	90.2 (2.4)	0.3 (0.04)	7.7 (0.4)	98.3
18	AAS27-D6-M1-P3 KAMACITE	68x43	4	92 (3.4)	0.5 (0.06)	6.4 (0.4)	98.8
19	AAS27-D6-M1-P5 KAMACITE	89x54	5	88.8 (0.9)	0.5 (0.1)	6.2 (1)	95.5
20	AAS27-D6-M3-P2 KAMACITE	54x65	3	89.1 (1)	0.5 (0.1)	7.4 (0.2)	97.0
21	AAS27-D6-M3-P2 - taenite inclusion	13	5	68 (2.5)	0.1 (0.1)	30.7 (1.8)	98.8
22	AAS27-D6-M5-P4 KAMACITE	78x55	5	89.3 (2.9)	0.5 (0.1)	9 (0.6)	98.7
23	AAS27-D6-M6-P2 KAMACITE	57x81	5	86.4 (3.7)	0.2 (0.1)	5.7 (0.3)	92.3
24	AAS27-D6-M6-P6 KAMACITE	79.9x130	6	92.9 (6.9)	0.6 (0.3)	7.4 (3.1)	100.9
25	AAS27-D6-M6-P7 KAMACITE	31x52	10	94.7 (1.2)	0.5 (0.1)	5.8 (1.1)	101.0
26	AAS27-D6-M6-P10 KAMACITE	82x13	8	94.9 (3.9)	0.6 (0.1)	2.4 (2.6)	97.9
27	AAS27-D6-M6-P12 KAMACITE	68x84	3	89.4 (4.7)	0.3 (0.04)	7 (0.4)	96.7
28	AAS27-D6-M7-P11 KAMACITE	104x133	8	88.8 (1.5)	0.5 (0.1)	7.3 (0.2)	96.6
29	AAS27-D6-M8-P2 KAMACITE	31x36	6	89.4 (2.2)	0.7 (0.1)	6.1 (0.3)	96.2
30	AAS27-D6-M8-P6 KAMACITE	50x51	9	89.7 (1)	0.2 (0.1)	6.3 (0.5)	96.2
31	AAS27-D6 M8-P8KAMACITE	44x62	3	90.09 (2.70)	0.03 (0.04)	4.74 (0.1)	94.9
32	AAS27-D6-M9-P6 KAMACITE	34x37	5	88.9 (2)	0.4 (0.06)	9.2 (0.4)	98.5
33	AAS27-D6-M11-P1 KAMACITE	20x47	6	88.5 (3.9)	0.3 (0.1)	7.8 (0.7)	96.6
34	AAS27-D6-M12-P2 KAMACITE	54x67	5	90.2 (3.1)	0.5 (0.1)	7 (0.6)	97.7
35	AAS27-D6-M14-P1 KAMACITE	177x197	6	89 (3.1)	0.5 (0.1)	6.2 (1.4)	95.6
36	AAS27-D6-M14-P4 KAMACITE	318x373	4	91.7 (3.1)	0.5 (0.1)	6.5 (1.4)	98.7
37	AAS26-D9-M2-P4 KAMACITE	36x38	8	87.4 (0.7)	0.5 (0.1)	7.6 (0.2)	95.5
38	AAS26-D9-M2-P7 KAMACITE	63x43	8	89.6 (1)	0.4 (0.1)	5.8 (0.4)	95.8
39	AAS26-D9-M2-P11 KAMACITE	44x92	13	89.5 (0.8)	0.7 (0.1)	5.4 (0.4)	95.5
40	AAS26-D9-M2-P14 KAMACITE	75x47	4	85.8 (1.6)	0.4 (0.1)	6.7 (0.8)	92.9
41	AAS26-D9-M2-P17 KAMACITE	48x55	5	84.6 (0.9)	0.6 (0.1)	9.8 (0.8)	94.9
42	AAS26-D9-M2-P20 KAMACITE	28	10	89.7 (2.6)	0.3 (0.1)	4.4 (1.6)	94.4
43	AAS26-D9-M2-P21 KAMACITE	53x35	2	84.9 (5)	0.3 (0.1)	3.7 (0.6)	88.9

44	AAS26-D9-M3-P21 KAMACITE	357x241	3	88 (1.2)	0.7 (0.1)	5.8 (0.2)	94.4	
45	AAS26-D9-M5-P9 KAMACITE	79x112	3	87.4 (2)	0.3 (0.2)	6.3 (1.9)	94.0	
46	AAS26-D9-M6-P6 KAMACITE	40x24	5	89.8 (1.1)	0.7 (0.1)	6.2 (1.2)	96.7	
47	AAS27-D6-M2-P2 KAMACITE	61x88	4	90.7 (3.6)	0.2 (0.1)	6.6 (1.3)	97.6	
48	AAS27-D6-M6-P6 KAMACITE	80x130	6	92.9 (6.9)	0.6 (0.3)	7.4 (3.1)	100.9	
49	AAS27-D6-M6-P12 KAMACITE	69x86	3	89.4 (4.7)	0.3 (0.02)	7 (0.4)	96.7	
50	AAS26-D9-M3-P3 KAMACITE	107x53	7	87.9 (2)	0.5 (0.1)	6.8 (2.5)	95.2	
51	AAS26-D9-M5-P1 KAMACITE	275x58	9	83.8 (1.2)	0.7 (0.1)	9.4 (0.5)	93.9	
52	AAS27-D6-M9-P3 KAMACITE	26x38	6	88.8 (2.16)	0.4 (0.14)	10 (0.72)	99.2	
53	AAS26-D37-M4-P10 KAMACITE	50x36	5	84.7 (1.1)	0.4 (0.1)	8.3 (0.2)	93.4	
54	AAS26-D37-M2-P3 PLESSITE	29x26	6	79.7 (1)	0.9 (0.1)	18.2 (0.5)	98.7	
55	AAS26-D37-M3-P3 PLESSITE	101	5	83.6 (2.2)	0.6 (0.1)	12.2 (0.5)	96.5	
56	AAS26-D37-M3-P24 PLESSITE	120x95	3	77.4 (0.8)	0.5 (0.3)	9.5 (5.9)	87.3	
57	AAS26-D37-M6-P3 PLESSITE	40x31	11	80.5 (3.2)	0.9 (0.1)	17.9 (2.1)	99.3	
58	AAS26-D36-M4-P3 PLESSITE	39x64	8	84.9 (2.9)	0.6 (0.1)	13.2 (1)	98.8	
59	AAS27-D6-M1-P7 PLESSITE	37x59	4	82.4 (1.9)	0.6 (0.1)	14.7 (1.7)	97.7	
60	AAS27-D6-M8-P1 PLESSITE	51x68	11	83.8 (1.7)	1 (0.2)	13.9 (0.5)	98.6	
61	AAS27-D6-M2-P1 KAMACITE-PLESSITE	30x59	12	92.5 (7.1)	0.4 (0.2)	7.8 (5.3)	100.7	
62	AAS 26-D9 M7-P1	PLESSITE	89x98	5	83.8 (2.6)	0.7 (0.2)	9.4(2.6)	93.9
63	AAS26-D37-M1-P16 PLESSITE	23x30	8	81.4 (2.7)	0.8 (0.1)	13 (2.4)	95.2	
64	AAS26-D37-M6-P6 TAENITE	124x45	21	58.9 (8)	0.15 (0.1)	37.1 (15.4)	96.2	
65	AAS26-D36-M1-P4 TAENITE	65x34	18	50 (2.5)	2 (0.2)	47.9 (2.7)	99.9	
66	AAS26-D36-M2-P1 TAENITE	132x185	13	73.7 (5.3)	0.2 (0.1)	25.7 (4.8)	99.6	
67	AAS26-D36-M2-P4 TAENITE	28x88	8	64.7 (2.9)	0.1 (0.1)	33.7 (2.4)	98.5	
68	AAS26-D36-M2-P5 TAENITE	131x95	9	59.3 (24)	0.1 (0.1)	40.7 (23)	100.0	
69	AAS27-D6-M4-P5 TAENITE	20x32	4	52.6 (4.7)	1.3 (0.5)	44.8 (14.7)	98.6	
70	AAS27-D6-M6-P8 TAENITE	15x25	1	66.30	1.6	30.90	98.8	
71	AAS27-D6-M6-P9 TAENITE	30x31	1	73.50	0.6	20.00	94.1	
72	AAS27-D6-M7-P9 TAENITE	169x175	13	82.6 (9.2)	0.9 (0.5)	19.4 (11.5)	102.9	
73	AAS27-D6-M8-P5 TAENITE	63x100	21	66.3 (3.3)	0.3 (0.1)	34.4 (12.4)	100.9	
74	AAS27-D6-M8-P7 TAENITE	25x69	5	56.5 (10.9)	0.05 (0.1)	42.4 (10.1)	99.0	
75	AAS27-D6-M8-P10 TAENITE	37x47	8	65.7 (10.6)	0.4 (0.3)	35 (10.3)	101.0	
76	AAS26-D9-M2-P6 TAENITE	89x73	1	65.60	1.4	30.50	97.5	
77	AAS26-D9-M2-P13 TAENITE	110x78	8	48.6 (1.6)	3.2 (0.1)	44.3 (1.6)	96.0	
78	AAS26-D9-M3-P7 TAENITE	97x74	9	61.5 (8.2)	0.2 (0.1)	37.5 (11.8)	99.2	
79	AAS26-D9-M5-P11 TAENITE	93x90	8	65 (5.7)	0.2 (0.1)	32.9 (5.4)	98.1	
80	AAS26-D9-M6-P3 TAENITE	65x52	7	76.2 (3.1)	1 (0.1)	22.2 (2.2)	99.4	

Table 2: Compositions of oxide rims surrounding metal micrometeorites and Fe-Ni beads

SAMPLE NO	PORTION ANALYZED	RIM THICKNES S (μm)	Fe ₂ O ₃	CoO	NiO	Total
AAS26-D37 M1-P13 KAMACITE		2.5	97.80	0.21	0.88	100.22
AAS26-D37M1-P15 KAMACITE	INNER RIM	2	98.15	0.30	1.64	100.84
	OUTER RIM	1.7	97.63	0.25	0.76	98.97
AAS26-D37-M2-P13 : KAMACITE		3	81.33	0.49	11.5 1	93.84
AAS26-D37-M3-P29 KAMACITE	INNER RIM	3.4	94.29	0.23	2.61	97.21
	OUTER RIM	2.5	96.98	0.08	0.47	97.56
AAS26-D37-M3-P53 KAMACITE	OUTER RIM	3	99.08	0.59	2.89	102.59
	INNER RIM	3	87.87	0.91	12.1 3	100.92
AAS26-D37-M4-P20 KAMACITE		5	91.40	0.23	0.79	92.33
AAS26-D37-M4-P21 KAMACITE		7.3	96.93	0.20	1.05	98.55
AAS26-D37-M4-P25 KAMACITE		2.4	89.94	0.37	6.88	97.19
AAS26-D37-M5-P4 KAMACITE		4.8	100.45	0.11	0.13	101.27
AAS26-D37-M6-P12 KAMACITE		5	98.79	0.44	1.31	100.54
AAS26-D36-M1-P2 KAMACITE		2.7	95.88	0.22	1.36	98.37
AAS26-D36-M2-P6 KAMACITE		4.4	99.59	0.12	1.30	101.28
AAS26-D6-M1-P3 KAMACITE		3.8	97.03	0.20	0.90	98.61
AAS26-D6-M1-P5 KAMACITE		5.4	96.19	0.17	1.79	98.25
AAS26-D6-M3-P2 KAMACITE		2	90.33	0.35	3.44	96.54
AAS26-D6-M5-P4 KAMACITE		5.6	102.08	0.23	0.99	103.50
AAS26-D6-M6-P6 KAMACITE		7.2	98.52	0.18	0.72	99.51
AAS26-D6-M6-P10 KAMACITE		6.9	96.02	0.54	1.57	99.04
AAS26-D6-M6-P12 KAMACITE		3.5	95.35	0.07	0.78	97.82
AAS26-D6-M8-P6 KAMACITE		5.7	93.55	0.06	0.80	97.41
AAS26-D6-M9-P6 KAMACITE		3.2	91.95	0.21	1.85	94.28
AAS26-D6-M12-P2 KAMACITE		4.3	92.58	0.49	6.37	102.77
AAS26-D6-M2-P2 KAMACITE		3.6	96.20	0.05	0.23	99.71
AAS26-D9-M3-P3 KAMACITE		2.7	96.51	0.15	0.58	97.24
AAS26-D9-M5-P1 KAMACITE		4.3	97.98	0.32	0.50	98.79
AAS26-D37-M3-P3 PLESSITE	OUTER RIM	1.2	95.17	0.24	1.68	97.12
	INNER RIM	1.6	97.54	0.23	4.11	101.98
AAS26-D6-M2-P1 KAMACITE-PLESSITE		2	91.08	0.36	5.49	99.41
AAS26-D37-M6-P6 TAENITE		3.4	86.98	0.16	6.82	93.97
AAS26-D36-M2-P1 TAENITE		3.6	77.11	0.10	5.16	97.40
AAS26-D36-M2-P5 TAENITE		2.3	93.51	0.00	4.49	98.25
AAS26-D6-M7-P9 TAENITE		5.2	99.27	0.17	0.65	100.26
AAS26-D6-M8-P5 TAENITE		3	90.51	0.22	7.51	98.23
AAS26-D9-M3-P7 TAENITE		4	67.53	0.16	29.1 8	96.86
AAS-26-D37-M4-P22 Fe-Ni bead		3.25	93.70	0.16	0.32	94.38

TABLE 3 : Chemical composition of unoxidized Fe-Ni beads

Serial No.	Sample No	Size μm	no of pts analyzed	Fe (2 σ)	Co (2 σ)	Ni (2 σ)	TOTAL
1	AAS26-D37-M1-P11	20	5	68.8 (1.9)	1.5 (0.2)	26.3 (1.1)	96.7
2	AAS26-D37-M3-P43	151	11	53 (0.6)	2.8 (0.1)	43.4 (0.7)	99.2
3	AAS26-D37-M6-P5	53	8	58.4 (2.2)	1.7 (0.1)	40.5 (1.5)	100.6
4	AAS27-D6-M7-P2	93	5	79.1 (3.7)	2.5 (0.1)	20.2 (1.1)	101.8
5	AAS27-D6-M8-P3	86	13	43.7 (2.1)	0.4 (0.1)	57.1 (2.1)	101.1
6	AAS27-D6-M13-P1	53	7	64.6 (1.7)	0.3 (0.04)	34.8 (2.4)	99.7
7	AAS-26-D37-M4-P22	22	3	81.1 (1.7)	0.6 (0.1)	9.6 (0.4)	91.3
8	AAS 27 D6 M6 P16	65	8	90.2 (3.2)	0.5 (0.1)	9 (0.6)	99.7
9	AAS-26-D36-M4-P4	64	3	93.15 (5.9)	0.2 (0.1)	6.2 (0.4)	99.6
10	AAS-26-D9-M3-P17	68	6	89.9 (0.9)	0.4 (0.1)	5.1 (1.8)	95.4
11	AAS 26-D9-M5-P8	31	4	87.2 (0.2)	0.4 (0.1)	5.7 (0.1)	93.3
12	AAS-26-D37-M3-P40	25	6	70.9 (0.2)	0.9 (0.1)	20.9 (0.1)	92.6
13	AAS-27-D6-M2-P3	61	9	76.9 (1)	1 (0.1)	24.4 (0.3)	102.3
14	AAS27-D6-M3-P4	39	12	50.8 (1.2)	3.2 (0.2)	46.2 (1.4)	100.2
15	AAS27-D6-M4-P2	66	8	70.2 (2.1)	2.1 (0.1)	27.6 (0.8)	100.0
16	AAS27-D6-M4-P4	24	8	56.6 (1.6)	1.7 (0.1)	41.8 (1.5)	100.0
17	AAS26-D9-M2-P10	43	7	30.6 (0.9)	0.6 (0.1)	67.8 (0.4)	99.1
18	AAS26-D9-M2-P22	39	4	84.3 (0.1)	0.5 (0.1)	10.6 (0.4)	95.4
19	AAS26-D9-M2-P23	27	4	83.5 (0.9)	1 (0.1)	11.6 (0.1)	96.1
20	AAS26-D9-M2-P25	62	7	69.9 (3.1)	1.2 (0.2)	26 (2.5)	97.0
21	AAS26-D9 M3-P19	95	4	49.6 (0.5)	0.3 (0.1)	47 (0.8)	96.8
22	AAS26-D9-M4-P1	26	3	31.2 (1)	2.2 (0.3)	59.3 (5.7)	92.7
23	AAS26-D9-M4-P4	28	3	35.1 (0.5)	0.4 (0.1)	60.1 (1.3)	95.5
24	AAS26-D9-M7-P4	59	7	75 (1)	1 (0.1)	20.3 (0.5)	96.3

TABLE 4 : Chemical composition of oxidized Fe-Ni beads

S.No.	Sample No.	Size μm	No of pts analyzed	Fe ₂ O ₃ (2 σ)	CoO (2 σ)	NiO (2 σ)	Total
1	AAS27-D6-M6-P1-P9	132	1	40.30	0.04	51.8	101.2
2	AAS26-D37-M2-P9	48	8	90.9 (1.6)	0.5 (0.1)	6.6 (1.1)	98.1
3	AAS26-D37-M2-P12	93	12	102.3 (2.8)	0.3 (0.1)	1.05 (1.4)	103.7
4	AAS27-D6-M1-P1	68	5	86.3 (4.1)	0.4 (1.4)	5 (2.3)	92.4
5	AAS27-D6-M1-P2	63	2	92.6 (1)	0.4 (0.1)	5 (1.1)	99.2
6	AAS27-D6-M1-P6	194	4	89.8 (5.4)	0.5 (0.2)	7.1 (2.7)	98.7
7	AAS27-D6-M5-P7	70	2	93 (1.5)	0.4 (0.1)	6.1 (1.7)	99.6
8	AAS27-D6-M7-P1	213	6	87.8 (18.2)	0.5 (0.4)	4.9 (2.4)	99.6
9	AAS27-D6-M10-P6	85	11	94.2 (2.3)	0.4 (0.2)	5.2 (1.8)	99.8
10	AAS26-D37 SPHERULES L-P1	294	11	84.9(0.5)	0.45(0.1)	10.16 (0.4)	95.5
11	AAS26-D37-SPHERULES-T-P3	78	26	87.4 (5)	0.3 (0.3)	3.4 (4.7)	91.9
12	AAS26-D37-SPHERULES-T-P4	76	11	90.8 (2.4)	0.4 (0.1)	5.4 (2.6)	96.6
13	AAS26-D37-SPHERULES-T-P8	69	9	89 (2.2)	0.3 (0.2)	4.2 (1.1)	95.4
14	AAS26-D37-SPHERULES-T-P9	70	15	89.8 (3.4)	0.4 (0.1)	4.7 (1.4)	95.4
15	AAS26-D37-SPHERULES-T-P10	69	10	91.4 (4.6)	0.3 (0.4)	3.8 (4.7)	95.8
16	AAS26-D37-SPHERULES-T-P13	65	9	90.9 (4.3)	0.4 (0.1)	4.8 (3.1)	96.5
17	AAS26-D37-SPHERULES-T-P14	66	6	84.9 (13.4)	0.3 (0.2)	4.6 (1.7)	93.5
18	AAS26-D9-M1-P3	74	4	81.2 (4.1)	0.6 (0.3)	6.9 (3.7)	88.7
19	AAS26-D9-M2-P15	110	6	97.8 (1.6)	0.1 (0.1)	0.4 (1.3)	98.4
20	AAS26-D36-M1-P6	56	8	93.8 (3.6)	0.2 (0.1)	5.4 (2)	99.3
21	AAS26-D36-M3-P3	64	7	91.9 (4.7)	0.4 (0.2)	6.1 (3.8)	98.4
22	AAS26-D36-M7-P2	89	10	88.1 (5.3)	0.3 (0.1)	3.6 (0.4)	92.0
23	AAS26-D37-M5-P3	63	9	91.8 (3.7)	0.4 (0.2)	5.7 (2.8)	97.8
24	AAS26-D36-M2-P2	68	11	98.4 (10)	0.6 (0.6)	9.2 (17)	108.1
25	AAS26-D9-M2-P12	10	8	60.7 (1.5)	1.8 (0.1)	55.3 (2.7)	118.0
26	AAS26-D9-M5-P6	30	3	83.4 (23.4)	0.7 (1.2)	11.9 (19.9)	96.0

TABLE 5 : COMPOSITION OF HYDRATED PORTIONS OF KAMACITE, PLESSITE, TAENITE AND Fe-Ni BEADS

HYDRATED PORTION																
	TYPE	Na ₂ O	SiO ₂	Al ₂ O ₃	Fe ₂ O ₃	Mg O	NiO	CoO	CaO	P ₂ O ₅	K ₂ O	TiO ₂	Mn O	SO ₂	Cr ₂ O ₃	Total
AAS26-D37 M1-P13	KAMACITE	0.07	0.22	0.10	82.38	0.58	0.30	0.14	0.03	0.06	0.01	0.04	0.01	0.01	0.01	83.95
AAS27-D6 M8-P13	TAENITE	0.13	0.31	1.15	83.21	0.04	0.07	0.09	0.09	0.08	0.02	0.04	0.60	0.07	0.07	85.97
AAS27-D6 M6-P10	KAMACITE	0.04	0.58	2.99	87.87	0.01	0.60	0.22	0.02	0.01	bdl	0.01	0.06	bdl	bdl	92.40
AAS27-D6 M7-P2	PLESSITE	0.14	0.98	0.62	61.89	0.06	18.61	1.82	0.10	bdl	0.04	0.01	bdl	0.10	bdl	84.37
AAS27-D6 M8-P6	KAMACITE	0.21	1.10	0.33	76.46	0.48	6.71	0.31	0.76	0.02	0.10	0.05	0.09	0.17	0.03	86.81
AAS26-D36 M2-P5	TAENITE	0.12	1.19	0.95	68.07	0.05	20.88	0.10	0.30	bdl	0.01	0.01	0.04	0.09	0.02	91.82
AAS27-D6 M14-P4	KAMACITE	0.14	1.23	0.22	75.33	0.21	3.54	0.46	0.83	0.01	0.09	0.05	0.08	0.12	0.01	82.32
AAS26-D36 M4-P3	PLESSITE	0.17	1.77	0.77	70.33	0.22	8.59	0.47	0.26	bdl	0.03	0.01	0.15	0.04	bdl	82.81
AAS26-D36 M2-P2	OXIDISED BEAD	0.08	1.83	0.20	81.11	0.10	7.32	0.57	0.17	0.01	0.01	0.01	0.14	0.04	bdl	91.59
AAS27-D6 M4-P5	TAENITE	0.07	1.91	1.74	48.12	0.28	24.77	1.56	0.62	0.03	0.03	bdl	bdl	0.36	0.01	79.48
AAS27-D6 M5-P4	KAMACITE	bdl	2.12	0.10	91.00	0.11	0.23	0.08	0.24	0.09	0.09	0.01	0.01	bdl	0.19	94.25
AAS27-D6 M3-P1	TAENITE	0.10	2.46	1.43	81.14	0.15	1.21	0.22	0.32	bdl	0.04	0.02	0.03	0.02	bdl	87.14
AAS26-D36 M2-P6	KAMACITE	0.05	3.05	0.63	86.12	0.03	1.44	0.14	0.40	bdl	0.03	0.01	1.12	0.08	bdl	93.09
AAS26-D37 M3-P2	KAMACITE	0.34	3.13	0.96	64.49	0.36	5.80	0.21	0.89	0.38	0.30	0.04	bdl	0.18	1.91	78.99
AAS27-D6 M14-P1	KAMACITE	0.48	3.35	0.46	74.16	0.57	5.79	0.54	0.76	0.06	0.08	0.01	0.06	0.09	0.03	86.45
AAS 26-D9 M2-P13	TAENITE	0.21	4.83	4.48	78.66	0.37	0.98	bdl	0.43	0.25	0.07	0.05	0.67	0.25	1.15	92.41
AAS26-D37 M4-P21	KAMACITE	0.16	7.00	4.34	55.65	0.50	3.36	0.13	0.41	0.05	0.28	0.06	0.05	0.03	bdl	72.02
AAS26-D37 M3-P23	KAMACITE	0.19	7.29	0.88	59.05	2.11	0.97	0.08	0.72	0.43	0.22	0.03	bdl	0.11	0.07	72.14
AAS26-D37 M3-P24	PLESSITE	0.08	7.33	0.14	58.28	4.80	0.48	0.09	1.69	1.75	0.05	0.05	0.10	0.06	2.84	77.73
AAS27-D6 M1-P7	PLESSITE	1.17	7.35	3.91	59.11	0.47	8.29	0.51	0.85	0.12	0.72	0.02	0.05	0.31	0.10	82.99
AAS 26-D9 M2-P21	KAMACITE	0.08	8.90	3.25	68.43	0.80	1.16	0.09	0.68	0.50	0.02	bdl	0.13	0.21	bdl	84.25
AAS 26-D9 M2-P4	KAMACITE	0.07	9.22	3.95	59.58	0.22	0.38	0.08	1.36	0.72	0.11	0.03	0.03	0.15	0.08	76.00
AAS 26-D9 M5-P9	KAMACITE	0.05	10.42	2.26	69.38	0.83	1.41	0.06	0.70	0.67	0.02	bdl	0.03	0.20	0.02	86.05
AAS27-D6 M6-P2	KAMACITE	0.62	11.24	4.87	62.80	4.10	1.21	bdl	0.66	0.46	0.14	0.03	0.11	0.30	0.03	86.58
AAS27-D6 M9-P6	KAMACITE	0.42	11.87	1.87	58.62	1.32	4.40	0.01	1.11	1.42	0.47	0.01	0.23	0.50	0.03	82.28
AAS26-D37 SPHERULES L-P1	PLESSITE	0.89	14.11	2.37	55.87	0.47	1.18	0.11	1.34	1.03	0.62	0.02	0.01	0.06	0.03	78.11
AAS 26-D9 M2-P6	TAENITE	0.04	18.30	1.49	70.80	1.21	1.30	0.18	0.22	0.11	0.02	0.01	0.21	0.05	0.01	93.94
AAS26-D36 M2-P1	TAENITE	0.49	19.57	2.84	60.30	0.52	7.63	bdl	0.73	0.47	0.15	bdl	0.07	0.68	0.01	93.47
AAS 26-D9 M2-P7	KAMACITE	0.02	35.85	4.11	25.38	3.06	0.75	0.04	0.99	0.30	0.01	0.02	0.32	0.15	0.79	71.77

* bdl=below detection level

TABLE S1 SUPPLEMENTARY DATA: Variation in nickel contents of individual taenite grains

Corresponding “M-Plots” are given in Figure 3 and nickel diffusion plots in Figure 4

(1) AAS26-D37-M6-P6 TAENITE					
	Fe	Co	Ni	Total	
RIM	51.02	0.12	2.24	75.95	
	50.66	0.17	43.63	94.46	
	54.38	0.12	40.01	94.51	
	57.71	0.12	39.37	97.20	
	58.76	0.11	38.51	97.38	
	59.40	0.11	38.12	97.62	
	59.79	0.13	37.57	97.50	
	61.49	0.17	35.93	97.59	
	61.78	0.23	35.63	97.64	
	61.55	0.13	35.16	96.84	
	61.11	0.12	35.15	96.38	
	61.38	0.16	35.42	96.96	
	61.88	0.17	35.00	97.05	
	62.04	0.16	35.32	97.52	
	62.02	0.21	35.56	97.79	
	61.14	0.12	36.11	97.37	
	59.96	0.19	36.89	97.04	
	59.57	0.16	36.69	96.41	
	58.55	0.18	37.10	95.82	
	58.13	0.20	37.50	95.83	
	57.14	0.14	37.57	94.85	
	48.17	0.12	37.20	85.49	
RIM	60.84	0.13	5.36	93.97	
	Fe	Co	Ni	O	Total
RIM 1	51.02	0.12	2.24	22.57	75.95
rim2	60.84	0.13	5.36	27.64	93.97
(2) AAS26-D6-M7-P9 TAENITE					
	Fe	Co	Ni	TOTAL	
RIM	69.43	0.14	0.51		
	77.51	0.63	25.09	103.24	
	79.12	0.78	22.83	102.72	
	81.59	0.82	21.34	103.75	
	81.76	0.95	18.88	101.60	
	86.89	1.04	17.61	105.55	
	82.62	0.91	17.50	101.03	
	87.03	1.02	17.38	105.44	
	83.86	0.99	17.00	101.86	

	83.48	0.90	16.22	100.59	
	83.72	0.94	17.27	101.92	
	82.24	0.94	18.27	101.45	
	85.83	0.95	18.32	105.10	
	78.14	1.08	23.96	103.18	
RIM	68.34	0.34	1.29		
	Fe	Co	Ni	O	Total
RIM1	69.43	0.14	0.51	30.11	100.26
RIM2	68.34	0.34	1.29	30.25	100.68
(3) AAS26-D9-M3-P7 TAENITE					
	Fe	Co	Ni	TOTAL	
RIM	48.84	0.11	19.03	94.35	
	59.86	0.25	39.15	99.26	
	60.94	0.10	37.66	98.70	
	62.14	0.14	36.94	99.23	
	62.10	0.18	37.04	99.32	
	62.70	0.15	36.43	99.28	
	61.83	0.22	37.22	99.27	
	61.95	0.19	36.80	98.94	
	61.51	0.19	37.40	99.09	
	60.84	0.17	38.50	99.51	
AVERAGE	61.54	0.17	37.46	99.18	
RIM	47.23	0.12	22.93	97.06	
	Fe	Co	Ni	O	Total
RIM1	48.84	0.11	19.03	26.27	94.35
RIM2	47.23	0.12	22.93	26.67	97.06
(4) AAS26-D6-M8-P5 TAENITE					
	Fe	Co	Ni	TOTAL	
RIM	63.30	0.17	5.90		
	62.22	0.34	36.77	99.32	
	64.41	0.30	36.22	100.93	
	65.85	0.22	35.45	101.52	
	66.85	0.24	33.99	101.08	
	67.56	0.18	33.76	101.51	
	68.02	0.35	33.47	101.84	
	68.18	0.29	32.83	101.30	
	68.32	0.21	33.38	101.91	
	67.50	0.31	33.27	101.08	
	67.36	0.31	33.65	101.31	
	66.00	0.25	33.62	99.87	
	66.83	0.32	34.53	101.68	
	66.31	0.21	34.52	101.05	
	64.35	0.17	33.85	98.37	
	66.20	0.27	34.32	100.78	

	66.27	0.28	34.19	100.73		
	66.74	0.25	34.16	101.15		
	66.68	0.31	33.96	100.95		
	66.96	0.25	34.78	101.99		
	65.03	0.17	35.18	100.39		
	63.57	0.28	37.01	100.86		
RIM	63.48	0.13	5.49			
	Fe	Co	Ni	O	Total	
RIM1	63.30	0.17	5.90	28.97	98.51	
RIM2	63.48	0.13	5.49	28.99	98.25	